Japan). Agarose L03 was purchased from Takara Bio (Shiga, Japan), whereas, EtBr was purchased from Nippon Gene (Toyama, Japan), CH_3CH was from Kanto Chemical (Tokyo, Japan). Pseudohypericin (**5**) was obtained from Planta Natural Products (Vienna, Austria). A quartz reaction container for high-throughput ROS assay was constructed by Ozawa Science (Aichi, Japan).

4.2. UPLC analysis on SJW constituents

The concentration of each constituent in the SJW extract was determined using a Waters Acquity UPLC system (Waters, Milford, MA), which included binary solvent manager, sample manager, column compartment, and SQD connected with MassLynx software. An Acquity UPLC BEH C 18 column (particle size: 1.7 μm, column size: 2.1 × 50 mm; Waters) was used, and the column temperature was maintained at 40 °C. All SJW components, except for hyperoside (**12**) and isoquercitrin (**13**), were separated using a gradient mobile phase consisting of CH_3CN (A) and 5 mM NH_4OH_2 (B) with a flow rate of 0.25 mL/min. The gradient condition of mobile phase was 0–0.5 min, 5% A; 0.5–7 min, 5–90% A; 7–7.5 min, 95% A; and 7.5–8.0 min, 5% A. Isocratic mobile phase, consisting of 10% CH_3CN/90% $HClO_4$ (0.35%), was used for measurement of hyperoside (**12**) and isoquercitrin (**13**).

4.3. Irradiation conditions

In the irradiation experiments, each assay mixture was stored in an Atlas Suntest CPS + solar simulator (Atlas Material Technology LLC) equipped with a xenon arc lamp (1500 W) and a UV special filter. The irradiation test was carried out at 25 °C with an irradiance of 250 W/m^2 (300–800 nm).

4.4. ROS assay

Both singlet oxygen and superoxide, generated from photo-irradiated chemicals, were determined by a colorimetrical method in accordance with previous reports (Onoue et al., 2008b,d). Singlet oxygen was measured in an aqueous solution by spectrophotometrically monitoring the bleaching of RNO at 440 nm using imidazole as a selective acceptor of singlet oxygen. Samples, containing the compounds under examination, RNO (50 μM) and imidazole (50 μM) in 20 mM sodium phosphate buffer (NaPB) (pH 7.4), were irradiated with UVA/B and Vis light (250 W/m^2: 300–800 nm), and then the UV absorption at 440 nm was measured using a SAFIRE microplate spectrophotometer (TECAN, Männedorf, Switzerland). For the determination of superoxide, samples containing the compounds under examination and NBT (50 μM) in 20 mM NaPB were irradiated with the UVA/B and Vis light (250 W/m^2: 300–800 nm) for the indicated periods, and the reduction in NBT was measured by the increase in absorbance at 560 nm using a SAFIRE microplate spectrophotometer (TECAN).

4.5. Photosensitized peroxidation of linoleic acid

Linoleic acid (1 mM) suspended in 20 mM NaPB (pH 7.4) containing 0.05% Tween 20 was irradiated in the presence of the test compound (200 μM), and lipid peroxidation was measured using a TBA assay as described previously (Onoue et al., 2008c). Addition of 0.67% TBA dissolved in 20 mM NaPB (pH 7.4, 1 mL) and 10 μL of 1.0% BHT solution in glacial AcOH to the irradiated sample (500 μL) was followed by heating at 95 °C for 30 min. The mixture was extracted with 1-butanol (1 mL), and absorbance of the extract was measured at 532 nm for the determination of TBA-reactive substances (TBARS). A standard curve of 1,1,3,3-tetraethoxypropane was used to quantitate the amount of malondialdehyde produced.

4.6. DNA photocleavage

The irradiated samples contained pBR322 DNA (final concentration, 10 μg/mL) dissolved in Tris-acetate-EDTA (TAE) buffer (40 mM Tris, 20 mM boric acid, and 1 mM EDTA; pH 7.4) and the examined compounds at a final concentration of 200 μM. Irradiated plasmid pBR322 DNA was separated by electrophoresis (0.8% agarose gel in TAE buffer), stained with EtBr solution (0.5 μg/mL), and analyzed with image analyzing software Image J.

4.7. UV spectral analysis

Hyperforin (**3**), hypericin (**4**), and quercitrin (**16**) were individually dissolved in 20 mM sodium phosphate buffer (NaPB, pH 7.4) at a final concentration of 20 μM. UV–Vis absorption spectra were recorded with a JASCO V-560 double-beam spectrophotometer (JASCO, Tokyo, Japan) interfaced to a PC for data processing (software: Spectra Manager). Spectrofluorimeter quartz cells with 10 mm pathlength were employed.

4.8. Data analysis

For statistical comparisons, one-way analysis of variance (ANOVA) with pairwise comparison by Fisher's least significant difference procedure was used. A P value of less than 0.05 was considered significant for all analyses.

Acknowledgements

This work was supported in part by a Grant-in-Aid from the Food Safety Commission, Japan [No. 0807], a Health Labour Sciences Research Grant from The Ministry of Health, Labour and Welfare, Japan, and a Project of Shizuoka Prefecture and Shizuoka City Collaboration of Regional Entities for the Advancement of Technological Excellence, Japan Science and Technology Agency (JST).

References

Alderfer, J.L., Soni, S.D., Arakali, A.V., Wallace, J.C., 1993. UV irradiation of nucleic acids: characterization of photoproducts of thymidylyl-(3′→5′)-2′-deoxy-5-fluorouridine. Photochem. Photobiol. 57, 770–776.

Foote, C.S., 1991. Definition of type I and type II photosensitized oxidation. Photochem. Photobiol. 54, 659.

Ito, H., Kobayashi, E., Takamatsu, Y., Li, S.H., Hatano, T., Sakagami, H., Kusama, K., Satoh, K., Sugita, D., Shimura, S., Itoh, Y., Yoshida, T., 2000. Polyphenols from *Eriobotrya japonica* and their cytotoxicity against human oral tumor cell lines. Chem. Pharm. Bull. (Tokyo) 48, 687–693.

Lawvere, S., Mahoney, M.C., 2005. St. John's wort. Am. Fam. Physician 72, 2249–2254.

Linde, K., 2009. St. John's wort – an overview. Forsch. Komplementmed. 16, 146–155.

Moore, D.E., 2002. Drug-induced cutaneous photosensitivity: incidence, mechanism, prevention and management. Drug Saf. 25, 345–372.

Nahrstedt, A., Butterweck, V., 2010. Lessons learned from herbal medicinal products: the example of St. John's Wort (perpendicular). J. Nat. Prod. 73, 1015–1021.

Ohkawa, H., Ohishi, N., Yagi, K., 1979. Assay for lipid peroxides in animal tissues by thiobarbituric acid reaction. Anal. Biochem. 95, 351–358.

Onoue, S., Igarashi, N., Kitagawa, F., Otsuka, K., Tsuda, Y., 2008a. Capillary electrophoretic studies on the photogenotoxic potential of pharmaceutical substances. J. Chromatogr. A 1188, 50–56.

Onoue, S., Igarashi, N., Yamada, S., Tsuda, Y., 2008b. High-throughput reactive oxygen species (ROS) assay: an enabling technology for screening the phototoxic potential of pharmaceutical substances. J. Pharm. Biomed. Anal. 46, 187–193.

Onoue, S., Igarashi, N., Yamauchi, Y., Murase, N., Zhou, Y., Kojima, T., Yamada, S., Tsuda, Y., 2008c. In vitro phototoxicity of dihydropyridine derivatives: a photochemical and photobiological study. Eur. J. Pharm. Sci. 33, 262–270.

Onoue, S., Ochi, M., Gandy, G., Seto, Y., Igarashi, N., Yamauchi, Y., Yamada, S., 2010. High-throughput screening system for identifying phototoxic potential of drug candidates based on derivatives of reactive oxygen metabolites. Pharm. Res. 27, 1610–1619.

Onoue, S., Seto, Y., Gandy, G., Yamada, S., 2009a. Drug-induced phototoxicity; an early in vitro identification of phototoxic potential of new drug entities in drug discovery and development. Curr. Drug Saf. 4, 123–136.
Onoue, S., Seto, Y., Oishi, A., Yamada, S., 2009b. Novel methodology for predicting photogenotoxic risk of pharmaceutical substances based on reactive oxygen species (ROS) and DNA-binding assay. J. Pharm. Sci. 98, 3647–3658.
Onoue, S., Tsuda, Y., 2006. Analytical studies on the prediction of photosensitive/phototoxic potential of pharmaceutical substances. Pharm. Res. 23, 156–164.
Onoue, S., Yamauchi, Y., Kojima, T., Igarashi, N., Tsuda, Y., 2008d. Analytical studies on photochemical behavior of phototoxic substances; effect of detergent additives on singlet oxygen generation. Pharm. Res. 25, 861–868.
Schmitt, L.A., Liu, Y., Murphy, P.A., Petrich, J.W., Dixon, P.M., Birt, D.F., 2006. Reduction in hypericin-induced phototoxicity by *Hypericum perforatum* extracts and pure compounds. J. Photochem. Photobiol. B 85, 118–130.
Schulz, V., 2001. Incidence and clinical relevance of the interactions and side effects of Hypericum preparations. Phytomedicine 8, 152–160.
Schulz, V., 2006. Safety of St. John's Wort extract compared to synthetic antidepressants. Phytomedicine 13, 199–204.
Seelinger, G., Merfort, I., Schempp, C.M., 2008. Anti-oxidant, anti-inflammatory and anti-allergic activities of luteolin. Planta Med. 74, 1667–1677.
Siegers, C.P., Biel, S., Wilhelm, K.P., 1993. Phototoxicity caused by hypericum. Nervenheilkunde 12, 320–322.
Vandenbogaerde, A.L., Kamuhabwa, A., Delaey, E., Himpens, B.E., Merlevede, W.J., de Witte, P.A., 1998. Photocytotoxic effect of pseudohypericin versus hypericin. J. Photochem. Photobiol. B 45, 87–94.
Viola, G., Miolo, G., Vedaldi, D., Dall'Acqua, F., 2000. In vitro studies of the phototoxic potential of the antidepressant drugs amitriptyline and imipramine. Il Farmaco. 55, 211–218.
Wilhelm, K.P., Biel, S., Siegers, C.P., 2001. Role of flavonoids in controlling the phototoxicity of *Hypericum perforatum* extracts. Phytomedicine 8, 306–309.
Yu, H., Wolford, S.T., Kegode, R., Zhao, W., Osweller, G.D., 1996. Hypericin-induced phototoxicity in cultured fibroblasts and swine erythrocytes. Photochem. Photobiol. 64, 168–173.
Zou, Y., Lu, Y., Wei, D., 2004. Antioxidant activity of a flavonoid-rich extract of *Hypericum perforatum* L. in vitro. J. Agric. Food Chem. 52, 5032–5039.

The AAPS Journal, Vol. 13, No. 3, September 2011 (© 2011)
DOI: 10.1208/s12248-011-9292-7

Research Article

Combined Use of *In Vitro* Phototoxic Assessments and Cassette Dosing Pharmacokinetic Study for Phototoxicity Characterization of Fluoroquinolones

Yoshiki Seto,[1] Ryo Inoue,[1] Masanori Ochi,[1] Graham Gandy,[2] Shizuo Yamada,[1] and Satomi Onoue[1,3]

Received 28 April 2011; accepted 23 June 2011; published online 8 July 2011

Abstract. The present study aimed to develop an effective screening strategy to predict *in vivo* phototoxicity of multiple compounds by combined use of *in vitro* phototoxicity assessments and cassette dosing pharmacokinetic (PK) studies. Photochemical properties of six fluoroquinolones (FQs) were evaluated by UV spectral and reactive oxygen species (ROS) assays, and phototoxic potentials of FQs were also assessed using 3T3 neutral red uptake phototoxicity test (3T3 NRU PT) and intercalator-based photogenotoxicity (IBP) assay. Cassette dosing pharmacokinetics on FQs was conducted for calculating PK parameters and dermal distribution. All the FQs exhibited potent UV/VIS absorption and ROS generation under light exposure, suggesting potent photosensitivity of FQs. *In vitro* phototoxic risks of some FQs were also elucidated by 3T3 NRU PT and IBP assay. Decision matrix for phototoxicity prediction was built upon these *in vitro* data, taken together with outcomes from cassette dosing PK studies. According to the decision matrix, most FQs were deduced to be phototoxic, although gatifloxacin was found to be less phototoxic. These findings were in agreement with clinical observations. Combined use of *in vitro* photobiochemical and cassette dosing PK data will be useful for predicting *in vivo* phototoxic potentials of drug candidates with high productivity and reliability.

KEY WORDS: cassette dosing pharmacokinetic study; fluoroquinolones; phototoxicity; reactive oxygen species; 3T3 neutral red uptake phototoxicity test.

INTRODUCTION

Drug-induced phototoxicity is elicited after exposure of skin to photoreactive pharmaceutical substances and is triggered by exposure to sunlight (1,2). The phototoxicity can be categorized as photoirritation, photogenotoxicity, or photoallergy, and some drugs can cause all three types of phototoxicity (3). A number of efforts have been made to develop effective screening systems to evaluate photosensitive/phototoxic potential through analytical and biological methods, with the aim of predicting adverse effects in early phases of drug discovery processes (1,4,5). Previously, our group proposed *in vitro* assay systems to assess the phototoxic risk of newly synthesized drug candidates, including a reactive oxygen species (ROS) assay (6), a derivatives of reactive oxygen metabolites assay (7), a capillary gel electrophoresis-based photocleavage assay (8), and an intercalator-based photogenotoxicity (IBP) assay (9). In addition to these *in vitro* phototoxic assessment tools, combined use of photochemical/photobiological and pharmacokinetic (PK) data has also been proposed as a new screening strategy for predicting *in vivo* phototoxic risk (10).

In drug discovery, *in vivo* PK study is essential to evaluate the absorption, distribution, metabolism, excretion, and PK profiles of drug candidates. However, single-compound discrete PK studies are time and resource consuming because large numbers of drug candidates have to be examined. Additionally, a large number of animals have to be killed to obtain sufficient data of drug candidates in the discrete PK approaches. To reduce the number of animals killed and improve the throughput of *in vivo* PK experiments, a cassette dosing approach has been suggested (11) and applied to drug discovery (12,13). In cassette dosing PK study, cocktail administration to a single animal enables evaluation of the PK profiles of multiple compounds at the same time;

[1] Department of Pharmacokinetics and Pharmacodynamics and Global Center of Excellence (COE) Program, School of Pharmaceutical Sciences, University of Shizuoka, 52-1 Yada, Suruga-ku, Shizuoka 422-8526, Japan.
[2] Drug Safety Research and Development, Pfizer Global Research and Development, Ramsgate Rd., Sandwich CT13 9NJ, UK.
[3] To whom correspondence should be addressed. (e-mail: onoue@u-shizuoka-ken.ac.jp)

ABBREVIATIONS: 3T3 NRU PT 3T3, Neutral red uptake phototoxicity test; ACN, Acetonitrile; ANOVA, Analysis of variance; $AUC_{0-\infty}$, Area under concentration *versus* time curve; $AUMC_{0-\infty}$, Area under moment curve; C_{max}, Maximum concentration; CPFX, Ciprofloxacin; DMEM, Dulbecco's modified Eagle's medium; dsDNA, Double-stranded DNA; EBSS, Earle's balanced salt solution; EMEA, European Medicines Agency; FDA, Food and Drug Administration; FQ, Fluoroquinolone; GFLX, Gatifloxacin; IBP, Intercalator-based photogenotoxicity; k_{el}, Elimination rate constant; K_p, Value tissue to plasma concentration ratio; LFLX, Lomefloxacin; LVFX, Levofloxacin; MRT, Mean residence time; NBT, Nitroblue tetrazolium; NaPB, Sodium phosphate buffer; NFLX, Norfloxacin; OECD, Organisation for Economic Co-operation and Development; PBS, Phosphate-buffered saline; PIF, Photoirritation factor; PK, Pharmacokinetic; RNO, *p*-Nitrosodimethylaniline; ROS, Reactive oxygen species; SPFX, Sparfloxacin; $t_{1/2}$, Elimination half-life; T_{max}, Time to reach maximum level; TO, Thiazole orange; UPLC/ESI-MS, Ultra-performance liquid chromatography equipped with electorospray ionization mass spectrometry; UV, Ultraviolet; VIS, Visible light.

however, the highly productive PK approach has never been applied to evaluate *in vivo* phototoxic risk of compounds. The purpose of this study was to propose a high-throughput effective screening strategy to evaluate and compare *in vivo* phototoxic risk of multiple compounds by the combined use of photobiochemical and cassette dosing PK data.

In the present study, six fluoroquinolones (FQs), including norfloxacin (NFLX), ciprofloxacin (CPFX), levofloxacin (LVFX), gatifloxacin (GFLX), lomefloxacin (LFLX), and sparfloxacin (SPFX), were used as a model chemical series (Fig. 1). FQs, antibacterials, are well recognized to be a phototoxic chemical series (14), and the structure-phototoxicity relationships of FQs have been reported (15,16); substitution groups at the eight position play a key role on the phototoxic potential of FQs. Thus, the tested FQs were divided into three groups based on the substituent at the eight position of FQs in the present study, namely, free (NFLX and CPFX), non-halogenated (LVFX and GFLX), and halogenated (LFLX and SPFX) groups. To clarify the *in vivo* phototoxic risk of these FQ series, the photobiochemical properties and PK profiles of the FQs were examined. Photochemical properties of the FQs were evaluated with a focus on ultraviolet (UV) absorption for photoactivation and ROS generation for photoreactivity. Phototoxic potentials were assessed by 3T3 neutral red uptake phototoxicity test (3T3 NRU PT) for photoirritation and IBP assay for photogenotoxicity. Cassette dosing PK analyses of the FQs were also carried out, and PK parameters and tissue distribution of FQs with a focus on the skin were estimated.

MATERIALS AND METHODS

Chemicals

NFLX, CPFX, GFLX, LFLX, salmon sperm DNA, plasmid pBR322 DNA, imidazole, *p*-nitrosodimethylaniline (RNO), nitroblue tetrazolium (NBT), thiazole orange (TO), Tween 20, disodium hydrogen phosphate 12 water, and sodium dihydrogen phosphate dihydrate were obtained from Wako Pure Chemical Industries (Osaka, Japan). LVFX, SPFX, nalidixic acid, trypsin/EDTA solution, and neutral red were purchased from Sigma (St. Louis, MO, USA). Acetonitrile (ACN) and methanol were obtained from Kanto Chemical Co., Inc. (Tokyo, Japan). DMEM, new-born calf serum, PBS without Ca^{2+} and Mg^{2+}, EBSS without phenol red, penicillin/streptomycin solution were purchased from Invitrogen (Carlsbad, CA, USA).

UV Spectral Analysis

FQs were dissolved in 20-mM sodium phosphate buffer (NaPB; pH 7.4) at a final concentration of 20 μM. UV–VIS absorption spectra were recorded with a HITACHI U-2010 spectrophotometer (HITACHI, Tokyo, Japan) interfaced to a PC for data processing (software: Spectra Manager). A spectrofluorimeter quartz cell with 10-mm pathlength was employed.

Irradiation Conditions

FQs were stored in an Atlas Suntest CPS+ solar simulator (Atlas Material Technology LLC, Chicago, USA) equipped with a xenon arc lamp (1,500 W). A UV special filter was installed to adapt the spectrum of the artificial light source to natural daylight. The irradiation tests were carried out at 25°C with an irradiance of 250 W/m^2 (290–800 nm).

In a 3T3 NRU PT, UV BIO-SUN illuminator (Vilbert-Lourmat, Marne-la-vallee, France) was employed. The irradiation test was carried out with an irradiace of ca. 50 W/m^2 (320–800 nm).

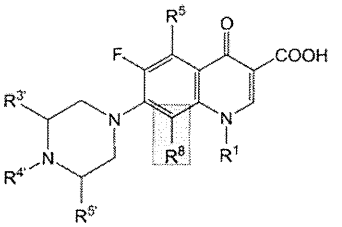

FQs	R^8	R^1	R^5	$R^{3'}$	$R^{4'}$	$R^{5'}$
Free group						
NFLX	−H	$-C_2H_5$	−H	−H	−H	−H
CPFX	−H		−H	−H	−H	−H
Non-halogenated group						
LVFX			−H	−H	$-CH_3$	−H
GFLX	$-OCH_3$		−H	$-CH_3$	−H	−H
Halogenated group						
LFLX	−F	$-C_2H_5$	−H	$-CH_3$	−H	−H
SPFX	−F		$-NH_2$	$-CH_3$	−H	$-CH_3$

Fig. 1. Structures of tested FQs

Determination of ROS

Both singlet oxygen and superoxide generated from irradiated chemicals were measured as we reported previously (17,18). Briefly, to monitor the generation of singlet oxygen, samples containing the compounds under examination, RNO (50 μM) and imidazole (50 μM) in 20 mM NaPB (pH 7.4), were irradiated with UVA/B and visible light, and then the UV absorption at 440 nm was measured using SAFIRE (TECAN, Männedorf, Switzerland). For the determination of superoxide, samples containing the compounds under examination and NBT (50 μM) in 20 mM NaPB (pH 7.4) were irradiated with UVA/B and visible light, and the reduction of NBT was measured by the increase in the absorbance at 560 nm using SAFIRE.

3T3 Neutral Red Uptake Phototoxicity Test

Balb/c 3T3 cells were maintained in culture for 24 h for formation of monolayers. Two 96-well plates per test chemical were then pre-incubated with eight different concentrations of the chemical for 1 h. One plate was then exposed to a dose of 5 J/cm^2 UVA (+Irr experiment) whereas the other plate was kept in the dark (−Irr experiment). The treatment medium was then replaced with culture medium and after 24 h, cell viability was determined by neutral red uptake for 3 h. Cell viability obtained with each of the eight concentrations of the test chemical was compared with that of the untreated controls, and the percent inhibition was calculated. For prediction of phototoxic potential, the concentration responses obtained in the presence and in the absence of UV irradiation were compared, usually at the IC_{50} level, *i.e.*, the concentration inhibiting cell viability by 50% of untreated controls. The photoirritancy factor (PIF) was determined:

$$PIF = \frac{IC_{50}(-Irr)}{IC_{50}(+Irr)}$$

IBP Assay

The photodynamic impairment of salmon sperm DNA by FQs was evaluated by IBP assay as reported previously (9). Briefly, in the irradiated group, each assay mixture (50 μL) in the 96-well microplate, containing the FQ (200 μM) and DNA (20 μg/mL) in 20 mM NaPB (pH 7.4), was irradiated with UVA/B and visible light for 45 min, and then TO was added to each well at a final concentration of 1.3 μM. As a control experiment, only 40 μL of the FQ in 20 mM NaPB (pH 7.4) was exposed to UVA/B and visible light, since photodegradants sometimes affect assay system. Then, DNA and TO were added to the sample at the same final concentration of irradiated experiments. In both irradiation and control experiments, each assay mixture (100 μL) was incubated at 37°C for 15 min to equilibrate intercalation of DNA with TO. To detect the intercalated TO, fluorescence (excitation, 509 nm and emission, 527 nm) was measured with SAFIRE.

In Vivo Preparations

Male Sprague–Dawley rats at 9 weeks of age (ca. 250–350 g, body weight) were purchased from SLC Inc. (Hamamatsu, Japan) and housed in the laboratory with free access to food and water, and maintained on a 12-h dark/light cycle in a room with controlled temperature (24±1°C) and humidity (55±5%). All the procedures used in the present study were conducted according to the guidelines approved by the Institutional Animal Care and Ethical Committee of the University of Shizuoka.

All FQs were dissolved in 0.1-M acetic acid/sodium acetic acid buffer (pH 4.8) containing 0.05% Tween 20. Rats were fasted for approximately 18 h before drug administration and received the cocktail solution containing all six FQs orally (5 mg/kg each).

Plasma Concentration of FQs After Oral Co-administration

Rats were anesthetized using pentobarbital (50 mg/kg) and then a guide cannula (PUC-40, EICOM Corp., Kyoto, Japan) was inserted into the jugular vein before the day when FQs was co-administered orally. Blood samples (approximately 150 μL) were collected from the cannulated jugular vein at the indicated times (0.083, 0.25, 0.5, 0.75, 1, 1.5, 2, 3, 4, 6, 9, and 12 h) after oral co-administration of FQs. Plasma obtained by centrifugation (10,000×g, 10 min, 4°C) was deproteinized by addition of ACN. The mixture was mixed for a few seconds and centrifuged (2,000 rpm, 1 min, 4°C). The supernatants were filtered and 50% ACN solution including nalidixic acid (5 μg/mL), an internal standard, was added to them (supernatant/nalidixic acid=9:1) for Ultra-performance liquid chromatography (UPLC) analysis.

Tissue Deposition of FQs After Oral Co-administration

At the indicated times (skin: 0.5, 1, 1.5, 2, 4, and 6 h; other tissues: 0.5 and 1 h) after oral co-administration of FQs, rats were killed by taking blood from the descending aorta under temporary anesthesia with diethyl ether, and the tissues were then perfused with cold saline from the aorta. The skin, liver, kidney, lung, cerebrum, cerebellum, white adipose, brown adipose, and eyes were dissected, and then fat and blood vessels were removed by trimming. The tissues were minced with scissors and homogenized in a Physcotron (Microtech Co., Ltd., Chiba, Japan) in 2 mL of ACN. The homogenates were transferred into stoppered test tubes. The tubes, which were used for homogenizing, were added to 2 mL of ACN for washing, and then the suspensions were also transferred into the stoppered test tubes. After shaking for 5 min and sonication for 10 min, the mixtures were centrifuged (3,500 rpm, 10 min). Extraction was repeated two times with ACN and the supernatants were pooled. The extraction was also repeated with 7 mL of Milli-Q and the supernatants were percolated through Waters Oasis HLB cartridges, which were preconditioned with 2 mL of methanol and 2 mL of Milli-Q. After the cartridges had been washed with 2 mL of Milli-Q (two times), the FQs were eluted with 4 mL of ACN. The collected eluents were pooled with ACN-extracts and the samples were evaporated to dryness under a gentle stream of nitrogen at 45°C. The residues were dissolved in deproteinized plasma solution including nalidixic acid (500 ng/mL) as an internal standard for UPLC analysis. The tissue to plasma concentration ratio (K_p value) was

calculated as the ratio of the tissue concentration of unchanged drug to the plasma concentration.

UPLC Analysis

The concentrations of FQs in rat tissues and plasma were determined with ultra-performance liquid chromatography equipped with electrospray ionization mass spectrometry (UPLC/ESI-MS) analysis. The UPLC/ESI-MS system consisted of a Waters Acquity UPLC™ system (Waters, Milford, MA, USA), which included a binary solvent manager, a sample manager, a column compartment, and a Micromass SQ detector connected with Waters Masslynx v 4.1. A Waters Acquity UPLC™ BEH C_{18} (particle size, 1.7 μm and column size, Φ 2.1×50 mm; Waters) was used, and column temperature was maintained at 40°C. The standards and samples were separated using a gradient mobile phase consisting of Milli-Q containing 0.1% formic acid (A) and methanol (B). The gradient condition of the mobile phase was 0–0.5 min, 80% A; 0.5–4 min, 80–25% A (gradient curve 8); 4–5 min, 5% A; and 5–6 min, 80% A, and the flow rate was set at 0.25 mL/min.

Pharmacokinetic Analysis

Pharmacokinetic characterization in the plasma was performed by non-compartmental analysis as implemented in WinNonlin Professional Version 5.2 (Pharsight Corporation, Mountain View, CA, USA) and that in skin was carried out by non-compartmental analysis. The elimination rate constant (k_{el}) was estimated by least square method from the terminal phase. The elimination half-life ($t_{1/2}$) was calculated using the following equation.

$$t_{1/2} = \frac{\ln 2}{k_{el}}$$

Area under concentration *versus* time curve ($AUC_{0\to\infty}$), area under moment curve ($AUMC_{0\to\infty}$), and mean residence time (MRT) were estimated using a trapezoid formula from 0 h to the last measurement time (T), after which the last observed concentration (C_T) and $t_{1/2}$ were used as follows:

$$AUC_{0\to\infty} = \int_0^T C\,dt + \frac{C_T}{k_{el}}$$

$$AUMC_{0\to\infty} = \int_0^T t \cdot C\,dt + \frac{T \cdot C_T}{k_{el}} + \frac{C_T}{k_{el}^2}$$

$$MRT = \frac{AUMC_{0\to\infty}}{AUC_{0\to\infty}}$$

where C is the observed plasma or skin concentration (plasma, ng/mL and skin, ng/g skin) and t equals the measurement time (h).

Data Analysis

For statistical comparisons, one-way analysis of variance (ANOVA) with pairwise comparison by Fisher's least significant difference procedure was used. A P value of less than 0.05 was considered significant for all analyses.

Standard error of each PK parameter in skin was defined by the delta method using the root of the following equation (19,20):

$$V(\overline{AUC}_{0\to\infty}) = \sum_{i=2}^{m}[(V(C_i)/n_i + V(C_{i-1})/n_{i-1}) \times ((t_i - t_{i-1})/2)^2] + (1/k_{el})^2 \cdot V(C_T)/n_T + (C_T/k_{el})^2 \cdot V(k_{el})/n_\lambda$$

$$V(\overline{AUMC}_{0\to\infty}) = \sum_{i=2}^{m}[(V(C_i)/n_i + V(C_{i-1})/n_{i-1}) \times ((t_i - t_{i-1})/2)^2] + (1/k_{el}^2)^2 \cdot V(C_T)/n_T + (C_T \cdot 2/k_{el}^3)^2 \cdot V(k_{el})/n_\lambda + (1/k_{el})^2 \cdot V(C_T)/n_T + (T \cdot C_T/k_{el}^2)^2 \cdot V(k_{el})/n_\lambda$$

$$V(\overline{MRT}) = \frac{V(\overline{AUMC}_{0\to\infty})}{(AUC_{0\to\infty})^2} + \frac{V(\overline{AUC}_{0\to\infty}) \cdot (AUC_{0\to\infty})^2}{(AUC_{0\to\infty})^4}$$

where m is the number of collection points, C_i is equal tothe skin concentration of FQs, t_i equals the collection time, and n_i represents the number of each collection time.

RESULTS

Photochemical Characterization of FQs

In the early stage of phototoxic events, photosensitive compounds initially have to absorb UVA/B radiation and then are transferred from ground state to excited state. According to the first law of photochemistry, measuring the UV-absorbing property of a chemical would be indicative of photoactivation. Then, the excited compounds attack biomolecules including proteins, lipids and DNA via direct or indirect processes, possibly leading to photoallergy, photoirritancy, and photogenotoxicity (6). In this study, the UV spectral patterns of the FQs were recorded in 20 mM NaPB (Fig. 2a). On the basis of the obtained UV spectral patterns, all the FQs exhibited strong absorption in the UVA/B range and only SPFX had a different absorption spectral pattern in the UV and visible light region. Their lowest energy bands in the UVA had maxima at 336 (NFLX), 335 (CPFX), 333 (LVFX), 334 (GFLX), 327 (LFLX), and 367 nm (SPFX) (Table I). The spectrum of solar radiation that reaches the surface of the earth is composed of visible light (400–700 nm), UVA (320–400 nm), and a part of UVB (290–320 nm) (21). On the basis of the present results and a previous report, all the FQs could be excited after absorption of photon energy from sunlight, and potentially causing photochemical reactions, possibly leading to phototoxic responses.

In the indirect phototoxic process, ROS are known as principal intermediate species, including singlet oxygen via type II photochemical reaction and superoxide via type I photochemical reaction. The ROS can cause phototoxic reactions, such as photoirritation, photogenotoxicity, and photoallergy, via oxidative reactions with biomolecules. Thus,

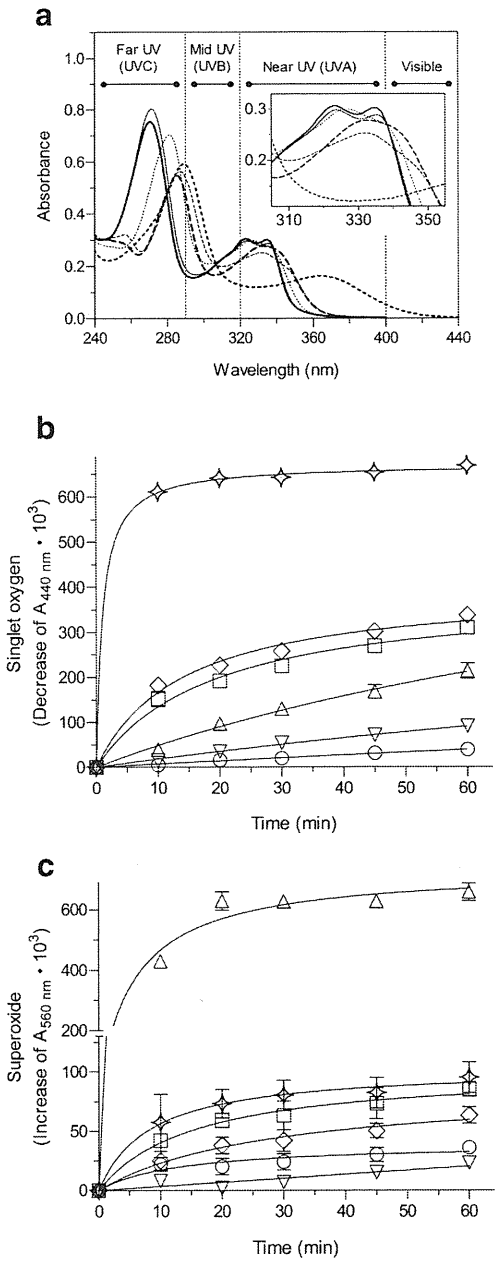

Fig. 2. Photochemical properties of FQs. UV-absorption spectra of FQs (20 μM) in 20 mM NaPB (pH 7.4) (**a**). *Thin solid line*, NFLX; *thick solid line*, CPFX; *thin dashed line*, LVFX; *thick dashed line*, GFLX; *thin dotted line*, LFLX; and *thick dotted line*, SPFX. Generation of singlet oxygen (**b**) and superoxide (**c**) from irradiated FQs (200 μM). The FQs were dissolved in 20 mM NaPB (pH 7.4) and then exposed to UVA/B light (250 W/m^2). *Empty squares*, NFLX; *empty diamonds*, CPFX; *empty triangles*, LVFX; *empty circles*, GFLX; *four-pointed stars*, LFLX; and *inverted empty triangles*, SPFX. Data represent mean±SD for three experiments

monitoring ROS generation from UV-exposed compounds may be useful to clarify the phototoxic potential of chemicals. In the present study, to clarify and compare the phototoxic potential of the FQs, the ROS assay on the FQs (200 μM) was carried out (Fig. 2b, c). All the FQs generated both singlet oxygen and superoxide, and, in particular, LFLX and LVFX have potent ability to generate these ROS compared with the other FQs. The singlet oxygen-forming ability was ranked as follows: LFLX≫CPFX>NFLX>LVFX>SPFX>GFLX, and the descending order of superoxide-producing capacity was as follows: LVFX≫ LFLX>NFLX>CPFX>GFLX>SPFX (Table I). On the basis of the data obtained, LVFX and LFLX would be expected to induce potent phototoxic reactions after exposure to UV, whereas GFLX and SPFX would be expected to be less phototoxic.

Detailed Phototoxic Reactions of FQs

According to the results from ROS assay, most FQs were deduced to have phototoxic potential, and their detailed phototoxic reactions needed to be evaluated. Previously, a number of effective *in vitro* methodologies were developed to characterize the detailed phototoxic potential of chemicals (1,4,22), and our group also proposed several *in vitro* photogenotoxic assessment tools (8,9). In the present study, the photoirritant and photogenotoxic risks of FQs were also evaluated by 3T3 NRU PT and IBP assay, respectively.

3T3 NRU PT has been established as an alternative *in vitro* methodology to various *in vivo* phototoxic evaluations (23). The assay is the only photosafety test which has been recommended by OECD guideline and has been validated to international standards (24). The test can assess the cytotoxic effects of UVA-irradiated compounds on Balb/c 3T3 mouse fibroblast cell line by using a concentration-dependent reduction of the uptake of neutral red. In this investigation, the viability curves of FQs with or without irradiation were determined up to 500 μg/mL. Figure 3 shows representative cell viability curves of the 3T3 cells after exposure to GFLX and SPFX. At the tested concentration of GFLX, cytotoxicity was not observed without irradiation, and GFLX at the higher concentration (>ca. 25 μg/mL) had slight cytotoxicity after exposure to UVA light. The EC_{50} values of the GFLX-treated group with/without UVA irradiation were estimated to be 122.0 and 42.77 μg/mL, respectively, and these values provided a PIF value of 2.85 for GFLX. With respect to the SPFX-treated group, the higher concentration of SPFX exhibited cytotoxicity without UVA irradiation. On the other hand, cytotoxicity occurred at a lower SPFX concentration after exposure to UVA light, resulting in the enhancement of SPFX-induced cytotoxicity. The EC_{50} values of the SPFX-treated group with/without UVA irradiation were 221.5 and 7.772 μg/mL, and the PIF value of SPFX was calculated to be 28.5. The PIF values of the tested FQs are described in Table I. In the OECD guidelines, classification criteria based on PIF values are defined as three groups, including phototoxic molecules (PIF>5), mildly or probably phototoxic molecules (2<PIF<5) and non-phototoxic molecules (PIF< 2) (24). On the basis of the classification criteria, most FQs tested, except GFLX, were found to be phototoxic, and GFLX was evaluated as a mildly/probably phototoxic compound. The *in vitro* phototoxic potential of FQs was deduced as follows: LVFX>LFLX>SPFX>CPFX>NFLX>GFLX.

The IBP assay was developed as a high-throughput screening tool for evaluating the photogenotoxic potential of chemicals (9). The assay evaluates the photodynamic impairment of dsDNA by phototoxins on the basis of the differences of fluorescence emission from DNA-fluorescent intercalating dye complexes between control group and irradiated group. In the present study, the IBP assay was carried out on FQs to

Table I. Photochemical and Phototoxic Data on FQs

FQs	UV absorption[a] λ_{max} (nm) [$\varepsilon \times 10^4$ (M^{-1} cm^{-1})]	ROS generation[b] $^1O_2$ ($\Delta A_{440} \times 10^3$)	ROS generation[b] O_2^- ($\Delta A_{560} \times 10^3$)	3T3 NRU PT (PIF)	Decrease in intercalated TO (Δ% of vehicle)*
NFLX	324 [1.5], 336 [1.4]	310±10	85±6	>6.0	15*
CPFX	324 [1.5], 335 [1.5]	338±13	63±7	>10.0	15*
LVFX	333 [1.3]	214±17	657±29	73.1	13*
GFLX	334 [1.4]	39±4	36±3	2.9	10*
LFLX	327 [1.5]	668±7	95±13	>28.8	21*
SPFX	367 [0.8]	91±7	23±3	28.5	13*

*$P<0.05$, significant difference between the control and irradiated data of each FQ
[a] The wavelengths of λ_{max} were selected longer than the lower limit of UVB (290 nm)
[b] Data represent mean±SD for three experiments

clarify the photogenotoxic potential (Fig. 4). Compared with the control group of vehicle, the fluorescence emission in control groups of NFLX and CPFX slightly decreased, which suggested that these photolytes intercalate into DNA. A decrease of fluorescence emission was also observed in the irradiated groups of NFLX and CPFX, and was higher than that in control groups; the differencing fluorescence might be indicative of photodynamic DNA damage by NFLX and CPFX. In contrast, LVFX, GFLX, LFLX, and SPFX did not affect the intercalating behavior of TO in the control group; however, the fluorescence emission in the irradiated group was decreased owing to DNA damage by irradiated LVFX, GFLX, LFLX, and SPFX. According to the data obtained, all the FQs would have photogenotoxic potential. Previously, some compounds were shown to induce severe photodynamic impairment of DNA in the agarose gel electrophoresis-based photogenotoxicity assay, and their values of difference for intercalated levels of TO between irradiated and control groups were estimated at over 15% of that of vehicle (9). On the basis of the present results, NFLX, CPFX and LFLX were found to have strong photogenotoxic potential, and the descending order of decrease in intercalated TO level was shown to be as follows: LFLX>CPFX≒NFLX>LVFX≒SPFX>GFLX (Table I). According to the ROS and IBP data, there was an empirical correlation between the generation of singlet oxygen and the reduction of intercalated TO level. Previously, DNA comet assay (25) and DNA photocleaving test (26) also demonstrated photogenotoxic potential of some FQs. In the DNA comet assay, the photogenotoxic potential of LFLX was found to be much higher than that of CPFX (25). In addition, three FQs such as LFLX, CPFX and NFLX exhibited potent DNA photocleaving activity in plasmid pBR322 DNA, and the photogenotoxic potential was ranked as follows: LFLX>CPFX, NFLX (26). Thus, these previous findings were partly consistent with the results from the IBP assay on FQs. Some FQs, including enoxacin, NFLX, CPFX, LFLX, and SPFX, induce DNA damage after exposure to UV, the major mechanisms of which may involve generation of singlet oxygen, radical chain reaction, and formation of thymine cyclobutane dimers as described in previous reports (27,28). Considering the present findings and previous reports, irradiated FQ-induced DNA damage may mainly occur through type II photochemical reaction.

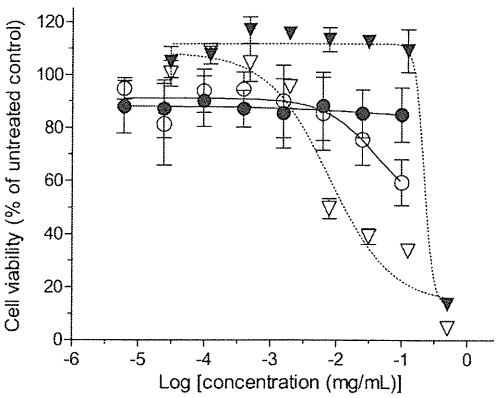

Fig. 3. Phototoxicity of representative FQs in the 3T3 NRU PT. The 3T3 cells were treated with different concentrations of GFLX or SPFX and irradiated with UVA light (50 kJ/m^2). Data represent mean±SD for two to six experiments. *Filled circles*, GFLX without UVA; *empty circles*, GFLX with UVA; *inverted filled triangles*, SPFX without UVA; and *empty squares*, SPFX with UVA

PK Assessments of FQs

Determination of the specific skin distribution of FQs would enable estimation of *in vivo* phototoxic risk; thus, PK profiling on FQs after oral administration was also carried

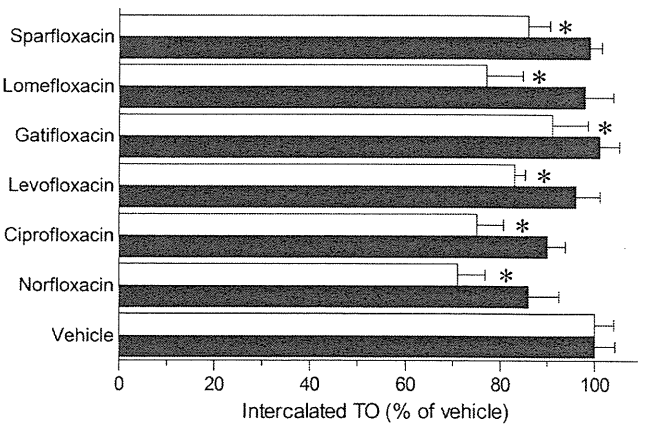

Fig. 4. DNA damage by irradiated FQs. Each drug (200 μM) was dissolved in 20 mM NaPB (pH 7.4) with/without DNA and then exposed to UVA/B light (250 W/m^2). TO solutions with/without DNA were added to the assay mixture, and fluorescence emitted from the TO-DNA complexes was measured. *Open bars*, UV irradiated; and *filled bars*, control group. Data represent mean±SD of four experiments. *$P<0.05$, significantly different from each control group

out. In the present study, cassette dosing PK analysis was used to improve the throughput of experiments and reduce the number of animals killed. After single cocktail oral administration of FQs (5 mg/kg), the concentration-time curves in the plasma and skin were obtained by UPLC/ESI-MS analysis (Fig. 5) and the PK parameters were calculated from the data obtained (Table II). With regard to the plasma concentration of FQs, all the FQs reached the maximum concentration (C_{max}) around 0.5 h after oral co-administration and the calculated C_{max} of plasma FQs was ranked as follows: LVFX>LFLX>GFLX>SPFX>CPFX>NFLX. As for the skin deposition of FQs, the times to reach maximum level (T_{max}) of FQs in the skin were ca. 0.5 h (NFLX) and ca. 1 h (other five FQs), and all T_{max} of skin FQs lagged behind each T_{max} of plasma FQs. The descending order of C_{max} of skin FQs was as follows: LFLX>GFLX>LVFX>SPFX>CPFX>NFLX. On the basis of the C_{max} of FQs, LFLX indicated the highest plasma and skin concentrations among the tested FQs at the same dose (5 mg/kg), and LFLX would be more likely to cause phototoxic reactions in the skin than the other FQs. In contrast, NFLX and CPFX might cause less phototoxic reactions in terms of their lower C_{max}. In addition to the C_{max} of the plasma and skin, the remaining potency of drugs would also be a key factor affecting the duration of

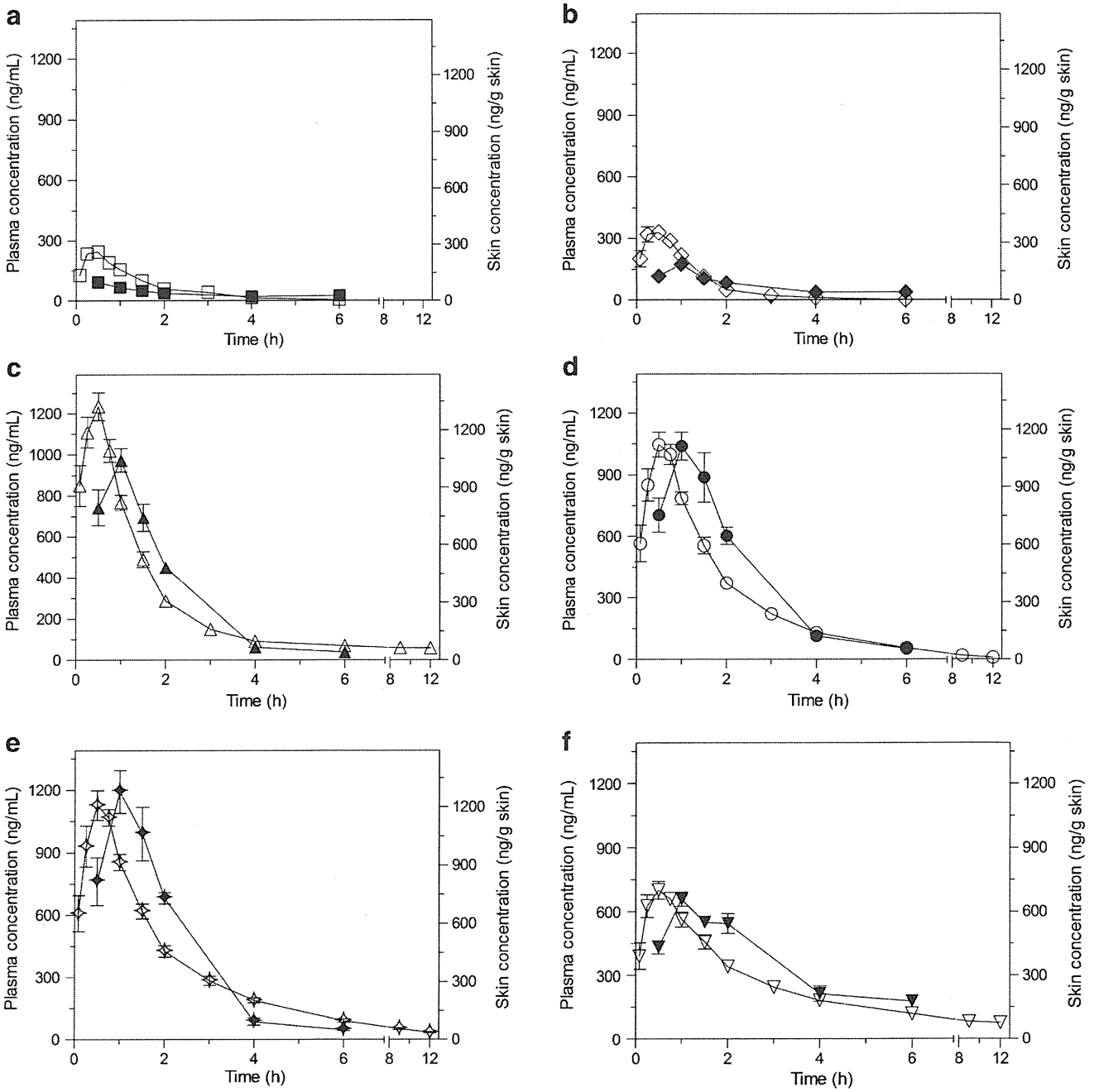

Fig. 5. Plasma and skin concentration-time profiles after oral co-administration of the FQs (5 mg/kg). **a** NFLX, **b** CPFX, **c** LVFX, **d** GFLX, **e** LFLX, and **f** SPFX. *Open symbols*, plasma and *filled symbols*, skin. Data represent mean±SE for six (plasma) and six to eight (skin) rats

Table II. Pharmacokinetic Parameters of FQs in the Plasma and Skin of Rats After Oral Co-administration

FQs	C_{max} (ng/mL or ng/g skin)	T_{max} (h)	$t_{1/2}$ (h)	MRT (h)
Plasma				
NFLX	257±27	0.38±0.06	0.98±0.09	1.51±0.11
CPFX	351±31	0.43±0.05	0.69±0.08	1.11±0.09
LVFX	1,270±52	0.46±0.04	1.23±0.05	3.01±0.20
GFLX	1,060±62	0.63±0.06	1.42±0.08	2.16±0.13
LFLX	1,150±66	0.58±0.05	1.48±0.03	2.88±0.07
SPFX	717±40	0.58±0.08	2.05±0.21	4.40±0.48
Skin				
NFLX	100±12	0.5	0.71±0.27	2.82±0.03
CPFX	187±14	1	0.59±0.14	2.58±0.01
LVFX	1,040±62	1	0.90±0.14	1.725±0.003
GFLX	1,110±72	1	1.34±0.38	1.995±0.003
LFLX	1,280±110	1	1.28±0.37	1.850±0.002
SPFX	658±33	1	1.99±0.86	3.638±0.006

Each value represents mean±SE for six (plasma) and six to eight (skin) rats

exposure risk of compounds to skin, a key trigger of phototoxicity; therefore, $t_{1/2}$ and MRT of the plasma and the skin were calculated. The $t_{1/2}$ of FQs was ranked as follows: SPFX>LFLX>GFLX>LVFX>NFLX>CPFX (in the plasma) and SPFX>GFLX>LFLX>LVFX>NFLX>CPFX (in the skin); the order of MRT was as follows: SPFX>LVFX>LFLX>GFLX>NFLX>CPFX (in the plasma) and SPFX>NFLX>CPFX>GFLX>LFLX>LVFX (in the skin). On the basis of these two parameters, SPFX had long-term exposure risk for the skin, and there is a possibility that the phototoxic events of SPFX persist over a longer time than the other FQs. Additionally, to clarify the selectivity of distribution property of the FQs, the tissue distribution for FQs at the T_{max} of skin concentration after oral co-administration was examined (Fig. 6) and the K_p values of the skin were estimated and ranked as follows: GFLX>LFLX>LVFX>SPFX>CPFX>NFLX. On the basis of the present results, skin and brown adipose are considered to be major sites for the distribution of the FQs, except for liver and kidney, during the early period after oral co-administration, and GFLX and LFLX are considered to be highly distributed in the skin.

DISCUSSION

In the present investigation, the combined use of photochemical and cassette dosing PK data on model FQs was shown to be an effective and productive screening strategy for evaluating *in vivo* phototoxic potential of the FQs. From the present photochemical and phototoxic data, most tested FQs, except GFLX, were found to have potent *in vitro* phototoxic risk whereas the phototoxic potential of GFLX was not too strong. The cassette dosing approaches could provide PK parameters and skin distribution properties of multiple FQs with high throughput. Focusing on the skin deposition of the FQs, LVFX, GFLX, and LFLX were highly distributed in the skin and SPFX had moderate and long-term exposure risk to skin. In contrast, the skin deposition properties for the free group, including NFLX and CPFX, demonstrated extremely low values.

Previously, a cassette dosing PK study was proposed for evaluating PK profiles of multiple compounds at the same time (11). Generally, multiple compounds are prepared at relatively low concentrations in the same solution, and the cocktail solution is administered to animals. Then, the blood and/or tissue concentrations of chemicals are determined by sensitive analytical methodologies, and PK parameters of chemicals are estimated on the basis of the data obtained. This approach has been applied to various administration routes, such as intravenous, intravitreal, and oral routes of administration, to aid drug discovery (12,29,30). Unlike a discrete PK study, in the cocktail dosing PK study, PK interactions on absorption, distribution, metabolism, and elimination might occur among tested chemicals. However, the cassette dosing approach also has attractive advantages such as high throughput and reduction of labor, animals killed, and other research resources (30). They might outweigh the disadvantages of cassette dosing approach at least for screening purpose since a large number of new drug candidates have to be examined in an early phase of drug discovery.

FQs, as a model chemical series, are clinically used as antimicrobial agents for treating various infections (31), the mechanism of which is inhibition of DNA gyrase, an essential bacterial enzyme, resulting in the suppression of DNA synthesis in microbes (32,33). In spite of the broad spectrum of antimicrobial activity, FQ-induced phototoxicity was also reported as an adverse effect in clinical trials (34). On the basis of this previous report, the halogenated group of FQs was shown to have severe *in vivo* phototoxicity, and the free group of FQs clinically exhibits mild photosensitivity. Non-halogenated FQs have less *in vivo* phototoxic potential than other types of FQs. However, the skin photosensitivity of GFLX was not observed in a double-blind, placebo- and positive-controlled study (35). In addition to the previous clinical trials, structure–activity and structure–side-effect relationships for FQs were examined in *in vitro* and *in vivo* phototoxic studies (36,37), and, in particular, the substituent groups at the eight position of FQs were reported to play a key role in phototoxicity of FQs on the basis of their structure-phototoxicity relationships (15,16). A halogen atom at the eight position exhibited potent phototoxic potential whereas a methoxy group at the eight position had less phototoxic potential. Thus, the order for phototoxic potential of FQ subseries is demonstrated as follows: halogenated FQs>free FQs>non-halogenated FQs.

In the present study, various photobiochemical data on FQs were initially obtained using *in vitro* phototoxic assessment tools, and the PK profiles of FQs were also estimated using the data from cassette dosing approaches. To integrate these data for *in vivo* phototoxic evaluation of the FQs, a decision matrix was built upon several experimental outcomes (Table III). The decision matrix is a summarized schematic model of qualitative or quantitative values, and it helps us to systematically identify, analyze, and evaluate the complicated sets of information. There are two crucial factors in the decision matrix, such as *in vitro* photobiochemical and

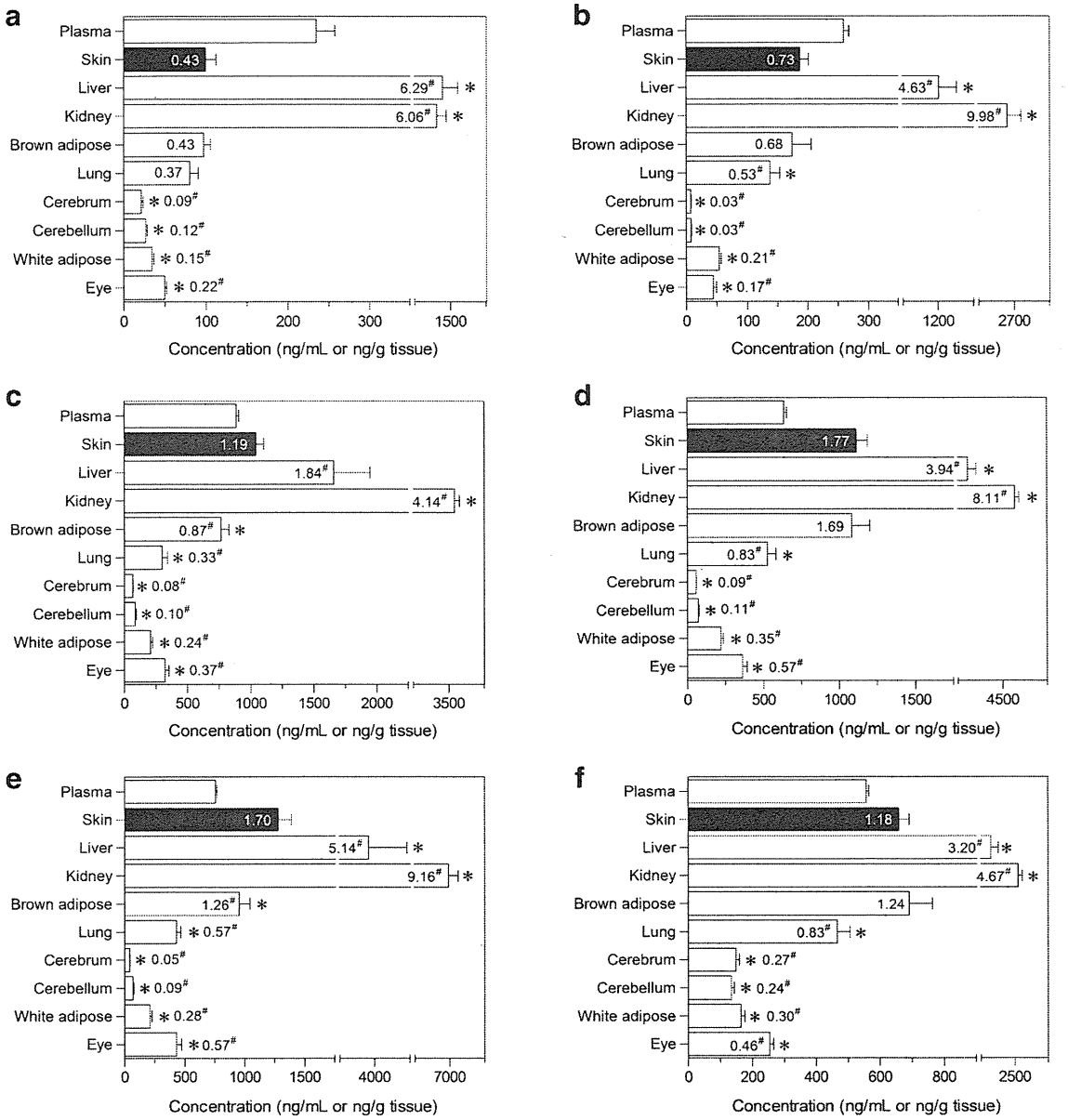

Fig. 6. Tissue distribution of FQs at the T_{max} of the skin after oral co-administration of the FQs (5 mg/kg). The mean of K_p values (mL/g tissue) is indicated in/near each column. **a** NFLX, **b** CPFX, **c** LVFX, **d** GFLX, **e** LFLX, and **f** SPFX. Each column represents mean±SE for eight rats. $^*P<0.05$, significantly different from each skin concentration. $^\#P<0.05$, significantly different from each K_p value of the skin

PK behaviors. When either of the two is at a low level, the tested chemical can be identified as mildly or less phototoxic. Of all PK parameters calculated, $t_{1/2}$ and MRT values in the skin should be of great importance since they were indicative of exposure period in the skin. On the basis of the phototoxic evaluation using the decision matrix, LFLX was deduced to have the most potent phototoxic risk because of its sensitive photoreactivity and high level in the skin, the mechanisms of which might include both photoirritation and photogenotoxicity mainly via type II photochemical reaction. LVFX would also have a potent phototoxic risk, especially photoirritancy, since both photoreacting and skin distribution properties were similar to those of LFLX except that LVFX had less photogenotoxic risk than LFLX. Compared with the present results on LFLX and LVFX, those on SPFX were indicative of moderate *in vitro* phototoxic risk and skin deposition; therefore, SPFX would also have phototoxic risk. Notably, the $t_{1/2}$ and MRT values for SPFX demonstrated the long-term exposure risk in the skin, and *in vivo* phototoxic risk of SPFX might persist longer. The PK profiles of GFLX were quite similar to those of LFLX; however, weak phototoxic behavior in the *in vitro* screenings suggested that GFLX might have limited phototoxic potential. From these findings, halogenated FQs tend to show phototoxic risk, although phototoxicity of non-halogenated FQ seemed to be variable depending on its chemical structure and *in vitro* photo-

Table III. Decision Matrix

		NFLX	CPFX	LVFX	GFLX	LFLX	SPFX
ROS generation	$^1O_2$ ($\Delta A_{440} \times 10^3$)	310	338	214	39	668	91
	O_2^- ($\Delta A_{440} \times 10^3$)	85	63	657	36	95	23
Phototoxic reactions	3T3 NRU PT (PIF)	>6.0	>10.0	73.1	2.9	28.8	28.5
	Decrease of intercalated TO (Δ% of vehicle)	15	15	13	10	21	13
PK profiles of skin	C_{max} (ng/g skin)	100	187	1,040	1,110	1,280	658
	K_p values (mL/g skin)	0.43	0.73	1.19	1.77	1.70	1.18
	$t_{1/2}$ (h)	0.71	0.59	0.90	1.34	1.28	1.99
	MRT (h)	2.82	2.58	1.72	1.99	1.85	3.64

Each crucial factor was divided into three levels. Black, gray and white cells represent high, moderate and low levels, respectively

reactivity. With respect to the free group of FQs, such as NFLX and CPFX, even if the free group had potent *in vitro* photoreactivity, it should have mild phototoxicity due to the lower migration to the skin than that of other groups at the present dosage (5 mg/kg). Overall, on the basis of the decision matrix, the order for the *in vivo* phototoxic risk of FQs was deduced as follows: LFLX>LVFX>SPFX>NFLX≒CPFX≫GFLX. In previous clinical reports, most tested FQs, including NFLX, CPFX, LVFX, LFLX, and SPFX, were reported to be phototoxic in clinical trials and the order for phototoxic potential was summarized as follows: LFLX>SPFX>CPFX>NFLX≒LVFX (34). As observed in the present study, cutaneous phototoxicity of GFLX was negligible in a clinical trial (35). The outcomes from the decision matrix approach were likely in agreement with the previous observations in clinical trials. From these findings, *in vivo* phototoxic risk of FQs could be estimated by combined use of *in vitro* photobiochemical and PK data.

For evaluating the phototoxic risk of new drug candidates, the European Medicines Agency (EMEA) and the Food and Drug Administration (FDA) established guidance on the photosafety testing of medical products, including phototoxicity (photoirritation), photogenotoxicity, photoallergy, and photocarcinogenicity tests (38–40). Both EMEA guidance and FDA guidance have similarly described test chemicals, which absorb light ranging from 290 to 700 nm (UVA/B and VIS) and are applied directly to the skin and/or eyes or are distributed in these sites after systemic administration; they also recommend 3T3 NRU PT as an *in vitro* phototoxicity test. 3T3 NRU PT was indicated by OECD guideline 432 in 2004 (24), and the test has become a general *in vitro* methodology for evaluating phototoxicity. Although the 3T3 NRU test can strongly detect the phototoxic potential of test chemicals, some positive chemicals in this test did not induce phototoxicity in *in vivo* phototoxicity tests in animals and/or human clinical photosafety studies (41). The overestimation of *in vitro* assessments such as 3T3 NRU PT might occasionally cause termination of development. Furthermore, the other contents of photosafety testing are markedly different between EMEA guidance and FDA guidance, and, in particular, EMEA guidance has no requirement of *in vivo* phototoxicity tests whether drug candidates have been determined as positive or negative in *in vitro* approaches. The assessment of photosafety for new drug candidates has not been completely elucidated yet, and more effective screening strategies for evaluating *in vivo* phototoxic risk are required. In the present study, the combined use of photobiochemical and PK data was proposed as one of the screening strategies for evaluating *in vivo* phototoxic risk of compounds, and the dermal PK data play a key role for better understanding of *in vivo* phototoxic potential.

In conclusion, *in vivo* phototoxicity of FQs could be evaluated by the combined use of photobiochemical and cassette dosing PK data. Additionally, the cassette dosing approaches would contribute to the improvement of throughput in PK analyses and save various resources. The present screening system would be an effective and high-throughput strategy for evaluating the *in vivo* phototoxic risk of new drug entities in an early stage of drug discovery.

ACKNOWLEDGMENTS

This work was supported in part by a Grant-in-Aid from the Food Safety Commission, Japan (no. 0807) and a Health Labour Sciences Research Grant from The Ministry of Health, Labour and Welfare, Japan.

REFERENCES

1. Onoue S, Seto Y, Gandy G, Yamada S. Drug-induced phototoxicity; an early *in vitro* identification of phototoxic potential of new drug entities in drug discovery and development. Curr Drug Saf. 2009;4(2):123–36.
2. Epstein S. The photopatch test; its technique, manifestations, and significance. Ann Allergy. 1964;22:1–11.
3. Epstein JH, Wintroub BU. Photosensitivity due to drugs. Drugs. 1985;30(1):42–57.
4. Henry B, Foti C, Alsante K. Can light absorption and photostability data be used to assess the photosafety risks in patients for a new drug molecule? J Photochem Photobiol B. 2009;96 (1):57–62.
5. Kleinman MH, Smith MD, Kurali E, Kleinpeter S, Jiang K, Zhang Y, *et al.* An evaluation of chemical photoreactivity and the relationship to phototoxicity. Regul Toxicol Pharmacol. 2010;58(2):224–32.
6. Onoue S, Tsuda Y. Analytical studies on the prediction of photosensitive/phototoxic potential of pharmaceutical substances. Pharm Res. 2006;23(1):156–64.
7. Onoue S, Ochi M, Gandy G, Seto Y, Igarashi N, Yamauchi Y, *et al.* High-throughput screening system for identifying phototoxic potential of drug candidates based on derivatives of reactive oxygen metabolites. Pharm Res. 2010;27(8):1610–9.
8. Onoue S, Igarashi N, Kitagawa F, Otsuka K, Tsuda Y. Capillary electrophoretic studies on the photogenotoxic potential of pharmaceutical substances. J Chromatogr A. 2008;1188(1):50–6.
9. Seto Y, Ochi M, Onoue S, Yamada S. High-throughput screening strategy for photogenotoxic potential of pharmaceutical substances using fluorescent intercalating dye. J Pharm Biomed Anal. 2010;52(5):781–6.
10. Seto Y, Onoue S, Yamada S. *In vitro/in vivo* phototoxic risk assessments of griseofulvin based on photobiochemical and pharmacokinetic behaviors. Eur J Pharm Sci. 2009;38(2):104–11.
11. Allen MC, Shah TS, Day WW. Rapid determination of oral pharmacokinetics and plasma free fraction using cocktail approaches: methods and application. Pharm Res. 1998;15 (1):93–7.
12. Smith NF, Raynaud FI, Workman P. The application of cassette dosing for pharmacokinetic screening in small-molecule cancer drug discovery. Mol Cancer Ther. 2007;6(2):428–40.
13. White RE, Manitpisitkul P. Pharmacokinetic theory of cassette dosing in drug discovery screening. Drug Metab Dispos. 2001;29 (7):957–66.
14. Przybilla B, Georgii A, Bergner T, Ring J. Demonstration of quinolone phototoxicity *in vitro*. Dermatologica. 1990;181(2):98–103.
15. Marutani K, Matsumoto M, Otabe Y, Nagamuta M, Tanaka K, Miyoshi A, *et al.* Reduced phototoxicity of a fluoroquinolone antibacterial agent with a methoxy group at the 8 position in mice irradiated with long-wavelength UV light. Antimicrob Agents Chemother. 1993;37(10):2217–23.
16. Matsumoto M, Kojima K, Nagano H, Matsubara S, Yokota T. Photostability and biological activity of fluoroquinolones substituted at the 8 position after UV irradiation. Antimicrob Agents Chemother. 1992;36(8):1715–9.
17. Kraljic I, Mohsni SE. A new method for the detection of singlet oxygen in aqueous solutions. Photochem Photobiol. 1978;28:577–81.
18. Pathak MA, Joshi PC. Production of active oxygen species ($^1O_2$ and O_2^{-}.) by psoralens and ultraviolet radiation (320–400 nm). Biochim Biophys Acta. 1984;798(1):115–26.
19. Takemoto S, Yamaoka K, Nishikawa M, Takakura Y. Histogram analysis of pharmacokinetic parameters by bootstrap resampling from one-point sampling data in animal experiments. Drug Metab Pharmacokinet. 2006;21(6):458–64.
20. Bailer AJ. Testing for the equality of area under the curves when using destructive measurement techniques. J Pharmacokinet Biopharm. 1988;16(3):303–9.
21. J Jagger. Why solar-ultraviolet photobiology? In: Solar-UV actions on living cells. New York: Plaeger Scientific. 1985;pp 1–10.
22. Spielmann H, Liebsch M, Doring B, Moldenhauer F. First results of an EC/COLIPA validation project of *in vitro* phototoxicity testing methods. ALTEX. 1994;11(1):22–31.
23. Liebsch M, Spielmann H. Currently available *in vitro* methods used in the regulatory toxicology. Toxicol Lett. 2002;127(1–3):127–34.
24. Organisation for Economic Co-operation and Development. OECD guideline for testing of chemicals, 432, *In vitro* 3T3 NRU phototoxicity test. Paris: Organization for Economic Cooperation and Development; 2004.
25. Chetelat AA, Albertini S, Gocke E. The photomutagenicity of fluoroquinolones in tests for gene mutation, chromosomal aberration, gene conversion and DNA breakage (Comet assay). Mutagenesis. 1996;11(5):497–504.
26. Condorelli G, de Guidi G, Giuffrida S, Miano P, Sortino S, Velardita A. Membrane and DNA damage photosensitized by fluoroquinolone antimicrobial agents: a comparative screening. Med Environ. 1996;24:103–10.
27. Vallet VL, Bosca F, Miranda MA. Photosensitized DNA damage: the case of fluoroquinolones. Photochem Photobiol. 2009;85(4):861–8.
28. Sauvaigo S, Douki T, Odin F, Caillat S, Ravanat JL, Cadet J. Analysis of fluoroquinolone-mediated photosensitization of 2'-deoxyguanosine, calf thymus and cellular DNA: determination of type-I, type-II and triplet-triplet energy transfer mechanism contribution. Photochem Photobiol. 2001;73(3):230–7.
29. He K, Qian M, Wong H, Bai SA, He B, Brogdon B, *et al.* N-in-1 dosing pharmacokinetics in drug discovery: experience, theoretical and practical considerations. J Pharm Sci. 2008;97(7):2568–80.
30. Proksch JW, Ward KW. Cassette dosing pharmacokinetic studies for evaluation of ophthalmic drugs for posterior ocular diseases. J Pharm Sci. 2008;97(8):3411–21.
31. Wolfson JS, Hooper DC. Fluoroquinolone antimicrobial agents. Clin Microbiol Rev. 1989;2(4):378–424.
32. Crumplin GC, Kenwright M, Hirst T. Investigations into the mechanism of action of the antibacterial agent norfloxacin. J Antimicrob Chemother. 1984;13(Suppl B):9–23.
33. Chow RT, Dougherty TJ, Fraimow HS, Bellin EY, Miller MH. Association between early inhibition of DNA synthesis and the MICs and MBCs of carboxyquinolone antimicrobial agents for wild-type and mutant [gyrA nfxB(ompF) acrA] *Escherichia coli* K-12. Antimicrob Agents Chemother. 1988;32(8):1113–8.
34. Lipsky BA, Baker CA. Fluoroquinolone toxicity profiles: a review focusing on newer agents. Clin Infect Dis. 1999;28 (2):352–64.
35. Grasela DM. Clinical pharmacology of gatifloxacin, a new fluoroquinolone. Clin Infect Dis. 2000;31 Suppl 2:S51–8.
36. Domagala JM. Structure-activity and structure-side-effect relationships for the quinolone antibacterials. J Antimicrob Chemother. 1994;33(4):685–706.
37. Hayashi N, Nakata Y, Yazaki A. New findings on the structure-phototoxicity relationship and photostability of fluoroquinolones with various substituents at position 1. Antimicrob Agents Chemother. 2004;48(3):799–803.
38. United States Department of Health and Human Services, Food and Drug Administration. Center for Drug Evaluation and Research (CDER) Guidance for Industry, Photosafety Testing. 2002.
39. The European Agency for the Evaluation of Medicinal Products, Evaluation of Medicines for Human Use, Committee for Proprietary Medicinal Products. Note for Guidance on Photosafety Testing, CPMP/SWP/398/01. 2002.
40. The European Agency for the Evaluation of Medicinal Products, Evaluation of Medicines for Human Use, Committee for Proprietary Medicinal Products. Concept Paper on the Need for Revision of the Note for Guidance on Photosafety testing, CPMP/SWP/398/01. 2008.
41. Lynch AM, Wilcox P. Review of the performance of the 3T3 NRU *in vitro* phototoxicity assay in the pharmaceutical industry. Exp Toxicol Pathol. 2011;63(3):209–14.

Journal of Pharmaceutical and Biomedical Analysis 55 (2011) 591–596

Contents lists available at ScienceDirect

Journal of Pharmaceutical and Biomedical Analysis

journal homepage: www.elsevier.com/locate/jpba

In vitro photobiochemical characterization of sulfobutylether-β-cyclodextrin formulation of bufexamac

Yoshiki Seto[a], Masanori Ochi[a], Naoko Igarashi[b], Ryo Inoue[a], Ami Oishi[a], Toshihiko Toida[b], Shizuo Yamada[a], Satomi Onoue[a,*]

[a] *Department of Pharmacokinetics and Pharmacodynamics and Global Center of Excellence (COE) Program, School of Pharmaceutical Sciences, University of Shizuoka, 52-1 Yada, Suruga-ku, Shizuoka 422-8526, Japan*
[b] *Graduate School of Pharmaceutical Sciences, Chiba University, 1-8-1 Inohana, Chuo-ku Chiba 260-8675, Japan*

ARTICLE INFO

Article history:
Received 13 January 2011
Received in revised form 16 February 2011
Accepted 19 February 2011
Available online 26 February 2011

Keywords:
Reactive oxygen species assay
Photoreactivity
Bufexamac
Sulfobutylether-β-cyclodextrin
Inclusion complex

ABSTRACT

The present study aimed to modulate the photoreactivity of bufexamac, with a focus on photostability and phototoxicity, by forming an inclusion complex with sulfobutylether-β-cyclodextrin (SBECD). The photobiochemical properties of bufexamac were evaluated by reactive oxygen species (ROS) assay and using *in vitro* photogenotoxic assessment tools. To assess the inclusion properties of SBECD complex with bufexamac, a UV absorption spectroscopic study was also carried out. The influence of SBECD on the photoreactivity of bufexamac was analyzed by ROS assay and photostability test. From the photobiochemical data, superoxide generation from irradiated bufexamac indicated its photoreactivity; however, the photogenotoxic risk of bufexamac was negligible owing to low DNA-binding affinity and DNA-photocleaving activity. SBECD complex of bufexamac was formed, and the association constant of the complex was calculated to be 620 M^{-1}. On the basis of the photochemical data on bufexamac co-existing with SBECD, ROS generation from irradiated bufexamac (200 μM) was inhibited by SBECD at concentrations of over 20 μM. The degradation constant of bufexamac in SBECD was decreased ca. 30% compared with that of bufexamac, suggesting improvement of its photostability. The phototoxic risk of bufexamac might be attenuated by SBECD complexation, and cyclodextrin inclusion complexes might be a useful approach for modulating the phototoxicity of drugs.

1. Introduction

Photochemical reactions of pharmaceutics, including photodegradation and phototoxicity, are severe problems in terms of stability and safety in the pharmaceutical industry, and their possible cascade has been reported [1,2]. Drugs are excited by UVA (320–400 nm) and UVB (290–320 nm), and then the drugs directly/indirectly react with molecules, resulting in photodegradation and phototoxicity [1]. Reactive oxygen species (ROS) have been reported as one of the major causative intermediate species for photochemical reactions [3], and the ROS generation from irradiated chemicals induce the oxidation of various molecules. Notably, excited compounds react with biomolecules, leading to phototoxic skin responses, including photoirritation, photoallergy, and photogenotoxicity [1,4]. Several classes of pharmaceuticals, such as diuretic agents [5], non-steroidal anti-inflammatory drugs (NSAIDs) [6], and tricyclic antidepressants [7], exhibit some or all of the phototoxic reactions. Recently, for evaluating the photoreactivity of pharmaceutics, a ROS assay was proposed as a new photochemical assessment tool [1,8] to monitor ROS generation from irradiated compounds, including both singlet oxygen and superoxide. There appeared to be a good relationship between ROS generation and occurrences of phototoxic events for a number of known phototoxic compounds [8].

In previous studies, inclusion complexes of drugs with cyclodextrins (CyDs) were used for modulating the photoreactivity of pharmaceutics, such as naproxen, amlodipine, flutamide and curcuminoids [9–12]. Notably, phototoxic skin reactions of topically administered drugs are a critical hazard, and the adverse effects should be avoided. Thus, CyD complexations might modulate the phototoxic risk of topically administered compounds. Bufexamac, the model compound in the present study (Fig. 1), is administered topically on the skin in clinical use; however, phototoxic skin event of bufexamac has been reported [13]. The purpose of the present study was to control the phototoxic potential of bufexamac by using complexation with sulfobutylether-β-cyclodextrin (SBECD), a β-CyD derivative. The photochemical behavior of bufexamac was assessed by ROS assay. For assessment of photogenotoxic potential, the interaction of bufexamac with DNA was assessed by circular dichroism (CD) analysis and DNA-binding assay [14] and

* Corresponding author. Tel.: +81 54 264 5633; fax: +81 54 264 5635.
E-mail address: onoue@u-shizuoka-ken.ac.jp (S. Onoue).

0731-7085/$ – see front matter © 2011 Elsevier B.V. All rights reserved.
doi:10.1016/j.jpba.2011.02.025

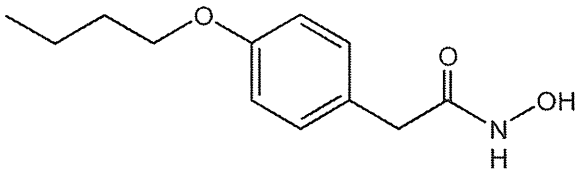

Fig. 1. Structure of bufexamac.

bufexamac-induced DNA photocleavage was evaluated by agarose gel electrophoresis. SBECD inclusion complex of bufexamac was formed and its inclusion properties were estimated using a spectroscopic study [15]. Possible changes of the photoreactivity of bufexamac with SBECD were evaluated by ROS assay, and the photostability of bufexamac with or without SBECD was monitored by ultra performance liquid chromatography equipped with electrospray ionization mass spectrometry (UPLC/ESI-MS).

2. Materials and methods

2.1. Chemicals

Bufexamac was purchased from Sigma (St. Louis, MO, USA). SBECD was supplied by Pfizer Inc. Salmon sperm DNA, plasmid pBR322 DNA, imidazole, p-nitrosodimethylaniline (RNO), nitroblue tetrazolium (NBT), Tween 20, disodium hydrogenphosphate 12-water, and sodium dihydrogenphosphate dihydrate were obtained from Wako Pure Chemical Industries (Osaka, Japan). Ethidium bromide (EtBr) and agarose L03 were, purchased from Nippon Gene (Toyama, Japan) and Takara Bio (Shiga, Japan), respectively. Acetonitrile was purchased from Kanto Chemical (Tokyo, Japan). A quartz reaction container for high-throughput ROS assay was constructed by Ozawa Science (Aichi, Japan).

2.2. Determination of reactive oxygen species (ROS)

Singlet oxygen was determined following the Kraljic and ElMoshni procedure [16]. Briefly, samples containing bufexamac with or without SBECD, RNO (50 μM), and imidazole (50 μM) in 20 mM sodium phosphate buffer (NaPB, pH 7.4) were irradiated with UVA/B (30,000 lx) in a Light-Tron Xenon (LTX-01, Nagano Science, Osaka, Japan), and then UV absorption at 440 nm was measured using a SpectraMax plus 384 microplate spectrophotometer (Molecular Devices, Kobe, Japan).

Superoxide anion was also determined according to the Pathak and Joshi procedure [17]. Samples containing bufexamac (free or in SBECD inclusion complex) and NBT (50 μM) in 20 mM NaPB (pH 7.4) were irradiated with UVA/B (30,000 lx) for the indicated periods, and the reduction of NBT was measured by the increase of their absorbance at 560 nm, using SpectraMax plus 384 microplate spectrophotometer.

2.3. Circular dichroism (CD) analysis of DNA

Salmon sperm DNA with or without bufexamac was dissolved in 20 mM NaPB (pH 7.4), and CD spectra (average of ten scans) were collected from samples (2.4 mL) at 0.4 nm intervals between wavelengths of 200 and 350 nm using a Jasco model J-600 spectropolarimeter. Measurement was carried out at room temperature, and a baseline spectrum was subtracted from the collected data.

2.4. DNA-binding assay

The affinity of drugs for salmon sperm DNA was determined by the competitive binding study. For competitive binding experiments, 10 μL of DNA solution at a concentration of 100 μg/mL, dissolved in 20 mM NaPB (pH 7.4), was mixed with 20 μL of the tested drug at various final concentrations ranging from 0 to 2 μM in a 96-well microplate (AGC TECHNO GLASS, Chiba, Japan), then 70 μL of EtBr (7.0 μM) was added to the assay mixture. The mixture was incubated for 15 min at 37 °C. After incubation, the fluorescence (excitation, 550 nm, and emission, 590 nm) of each mixture (100 μL) in 96-well microplates was measured with a Multilabel Counter (PerkinElmer, Norwalk, CT, USA).

2.5. DNA-photocleavage assay

The sample containing pBR322 DNA (10 μg/mL) and bufexamac (200 μM) in Tris–acetic acid–EDTA (TAE) buffer (40 mM Tris, 20 mM acetic acid, and 1 mM EDTA) was irradiated with UVA/B (375 kJ/m^2) in an Atlas Suntest CPS+ solar simulator (Atlas Material Technology LLC, Chicago, USA) equipped with a xenon arc lamp (1500 W). After the irradiation test, irradiated plasmid pBR322 DNA was separated by electrophoresis (0.8% agarose gel in TAE buffer), visualized with EtBr staining, and analyzed with image analyzing software Image J.

2.6. Determination of stoichiometry and the association constant

Bufexamac (0.5 mM) was dissolved in 20 mM NaPB (pH 7.4) containing 5% acetonitrile with SBECD (5, 10, 15, 20, 25, and 30 mM). Solutions containing the same concentrations of SBECD without bufexamac were also prepared. UV–Vis absorption spectra were recorded with a HITACHI U-2010 spectrophotometer (HITACHI, Tokyo, Japan) interfaced to a PC for data processing (Software: Spectra Manager). Spectrofluorimeter quartz cell with 10 mm pathlength was employed. The spectra of bufexamac were obtained by the subtraction of the spectra of SBECD from those of complex for removal of the contribution of SBECD. The obtained UV absorption of bufexamac at 278 nm (A_{278}) was substituted into the following Scott's equation, and described on Scott's plot [15]:

$$[\text{SBECD}] \cdot [\text{Buf}] \cdot \frac{L}{A_{278}} = \frac{1}{\varepsilon}[\text{SBECD}] + \frac{1}{K \cdot \varepsilon}$$

where [SBECD] and [Buf] indicate the molar concentrations of SBECD and bufexamac (mM), respectively. L is the light path length, ε equals to the molar extinction coefficient, and K represents the association constant. Then, the values of K and stoichiometry were obtained from Y-intercept/slope and linearity of Scott's plot, respectively.

2.7. Photostability testing

For photostability testing, the solutions of bufexamac (1 mg/mL) and its SBECD inclusion complex (equimolar ratio between bufexamac and SBECD) were dissolved in water containing 50% acetonitrile in a 1.5 mL clear glass vial (12 mm × 32 mm, Shimadzu, Kyoto, Japan). The samples were stored in the Atlas Suntest CPS+ solar simulator, and photostability testing was carried out at 25 °C with an irradiance of 750 W/m^2 for the indicated times (0, 15, 30, 60, and 120 min). The irradiated and non-irradiated samples were subjected to UPLC analyses to determine the amounts of remaining bufexamac. All analyses were performed on a Waters Aquity UPLC™ system (Waters, Milford, MA), which includes a binary solvent manager, a sample manager, a column compartment, and a Micromass SQ detector connected with a Waters Masslynx v 4.1. A Waters Acquity UPLC™ BEH C_{18} (particle size: 1.7 μm, column size: ϕ2.1 mm × 50 mm; Waters) was used, and the column temperature was maintained at 40 °C. The standards and samples were separated using a gradient mobile phase consisting of Milli-Q containing 0.1% formic acid (A) and methanol (B). The gradient condition of

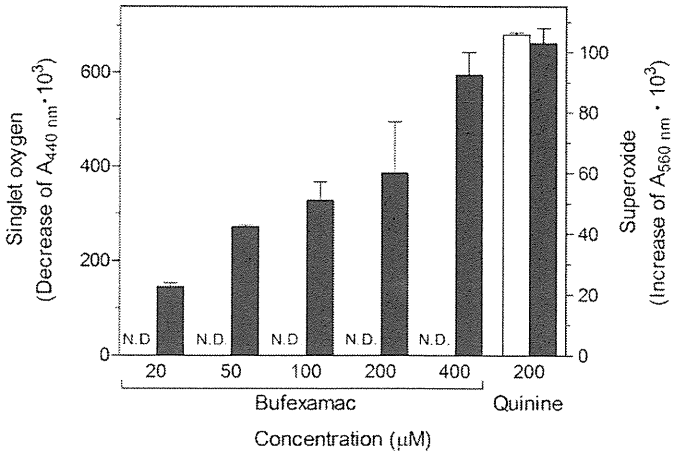

Fig. 2. Generation of ROS from photoirradiated bufexamac and quinine. Each chemical was dissolved in 20 mM NaPB (pH 7.4) at the indicated concentrations, and then exposed to simulated sunlight (30,000 lx). Open bar, singlet oxygen; and filled bar, superoxide. Data represent mean ± S.D. of three experiments.

the mobile phase was 0–0.5 min, 50% A; 0.5–3.5 min, 50–5% A; 3.5–5 min, 5%, and the flow rate was set at 0.25 mL/min.

2.8. Data analysis

For statistical comparisons, a one-way analysis of variance (ANOVA) with the pairwise comparison by Fisher's least significant difference procedure was used. A P value of less than 0.05 was considered significant for all analyses.

3. Results

3.1. Photochemical reactions of bufexamac

The ROS assay enabled to identification of the type of photochemical reaction by monitoring the generation of singlet oxygen through type II photochemical reaction and superoxide through type I photochemical reaction. In the present study, the generation of ROS from bufexamac was detected by ROS assay to clarify the type of photochemical reaction for bufexamac (Fig. 2). Exposure of quinine, a known phototoxic drug, to simulated sunlight resulted in the generation of both singlet oxygen and superoxide; however, bufexamac could generate only superoxide in a concentration-dependent manner. The results suggested that bufexamac would mainly induce type I photochemical reaction. The ROS-generating behavior of bufexamac ($^1O_2$, $\Delta_{440} \times 10^3$: not detected, O_2^-, $\Delta_{560} \times 10^3$: 60) was similar to that of carbamazepine ($^1O_2$, $\Delta_{440} \times 10^3$: not detected, O_2^-, $\Delta_{560} \times 10^3$: 96), a phototoxic drug [18], at a concentration of 200 μM [19]. Thus, bufexamac was found to be photoreactive and/or phototoxic, and the result was in agreement with a previous clinical report [13].

3.2. Photogenotoxic potential of bufexamac

For further photochemical characterization, the interaction of bufexamac with DNA was evaluated by DNA-binding assay [14], and nalidixic acid, which has the affinity to DNA, was used as a positive control (Fig. 3A). The emission of intense fluorescence from ethidium (4.9 μM) was observed in the presence of DNA (10 μg/mL). The addition of nalidixic acid induced a decrease of fluorescence in a concentration-dependent manner; however, no significant changes of fluorescence emission were observed for bufexamac, suggesting low affinity of bufexamac to DNA. To clarify the interaction of bufexamac and DNA, CD spectral analysis on DNA

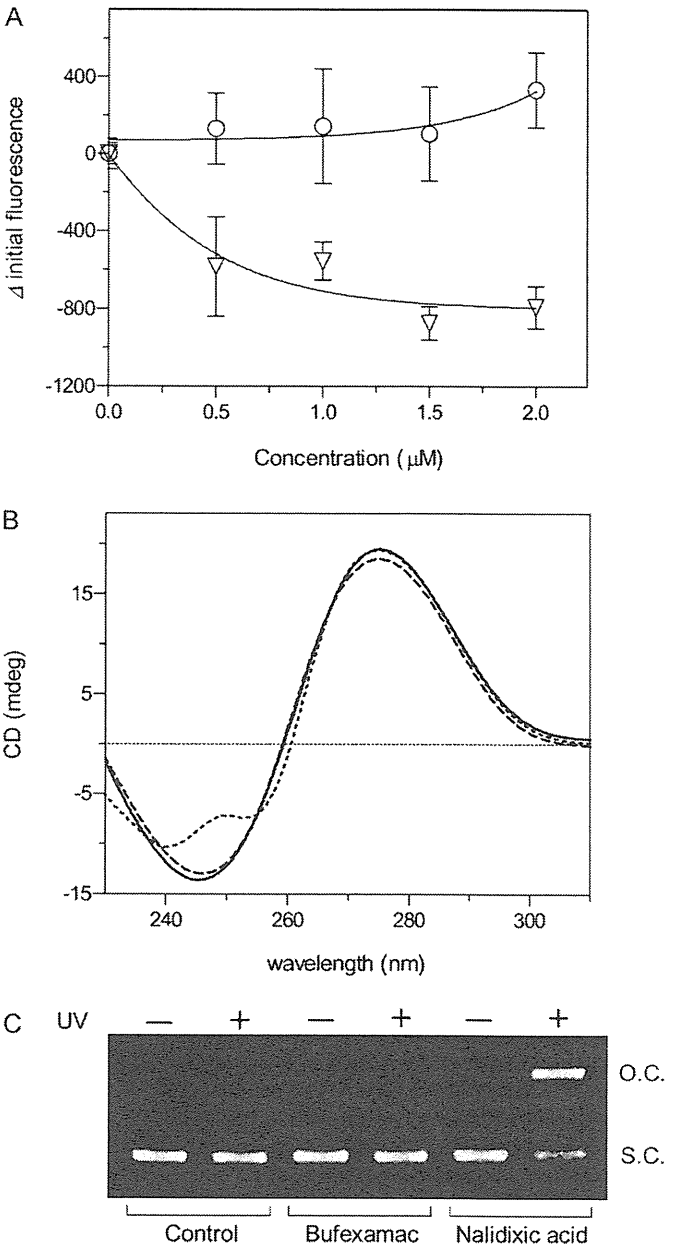

Fig. 3. *In vitro* photogenotoxic assessments. (A) Typical ethidium displacement curves for chemicals. The binding of ethidium (4.9 μM) to DNA was inhibited by increasing concentrations of nalidixic acid, but not by bufexamac. (○) Bufexamac and (▽) nalidixic acid. Data represent mean ± S.D. of four experiments. (B) CD spectra representative of DNA (100 μg/mL) in the presence of compounds (100 μM). Solid line, DNA alone; dashed line, DNA in the presence of bufexamac; and dotted line, DNA in the presence of nalidixic acid. (C) Photodynamic impairment of plasmid pBR322 DNA induced by irradiated compounds. Supercoiled DNA was exposed to UV with/without compounds. EtBr-stained 0.8% agarose gels are shown. O.C., open circular form; and S.C., supercoiled form.

(100 μg/mL) with or without compounds (100 μM) was also carried out (Fig. 3B). A solution of DNA exhibits a positive band at 275 nm due to base stacking and a negative band at 248 nm due to the helicity, which is characteristic of DNA in the right-handed B form [20]. Adding nalidixic acid to DNA solution, the intensity of the negative band at 248 nm decreased, suggesting the structural changes of DNA. In contrast, no spectral transitions were observed for bufexamac, suggesting weak interaction of bufexamac with DNA.

To validate the photogenotoxic risk of bufexamac, the conversion of plasmid pBR322 DNA from supercoiled (SC) form to open circular (OC) form was also analyzed by AGE (Fig. 3C). DNA damage

was clearly induced by nalidixic acid after exposure to simulated sunlight, and the conversion of pBR322 DNA from the SC to the OC form was estimated to be ca. 64% on the basis of the band intensity. In contrast, bufexamac-induced DNA photocleavage was not observed, suggesting that bufexamac is less photogenotoxic. Overall, bufexamac exhibited neither interaction with DNA nor DNA-photocleaving activity, and bufexamac may not cause photogenotoxicity.

3.3. Stoichiometric analysis of bufexamac–SBECD inclusion complex

The photobiochemical data of bufexamac indicated photodegradative and phototoxic potentials, except photogenotoxic risk, and SBECD complexation was applied for modulating the photoreactivity of bufexamac in this study. Generally, there is an optimal molar ratio between CyD and chemicals for forming an inclusion complex; therefore, a spectroscopic method using the changes of UV-absorption spectra and Scott's plot was used for evaluating the stoichiometry of the inclusion complex in the present investigation [15]. The UV spectral patterns of SBECD–bufexamac complex were recorded in 20 mM NaPB (pH 7.4) (Fig. 4A). On the basis of UV spectral data, hyperchromicity and slight bathochromicity were observed ranging from 250 nm to 300 nm, and strong absorption was detected at approximately 278 nm; these effects suggested that the UV absorbability of bufexamac was changed by SBECD. To obtain the stoichiometry and association constant of the SBECD inclusion complex of bufexamac, Scott's plot was described using the UV absorption data and the concentrations of bufexamac and SBECD (Fig. 4B). The plot of SBECD concentration versus [SBECD]·[Buf]/Absorbance exhibited linearity, and its correlation coefficient was estimated to be 1.00. Generally, the inclusion ratio between CyD and compound is stoichiometrically determined to be 1:1 when Scott's plot is indicative of the linearity [21]. In addition to the stoichiometry of the inclusion complex, the value of K of the inclusion complex was also calculated to be 620 M^{-1} from the present analysis. On the basis of the data obtained, SBECD forms a 1:1 inclusion complex with bufexamac, and the complex should be relatively stable.

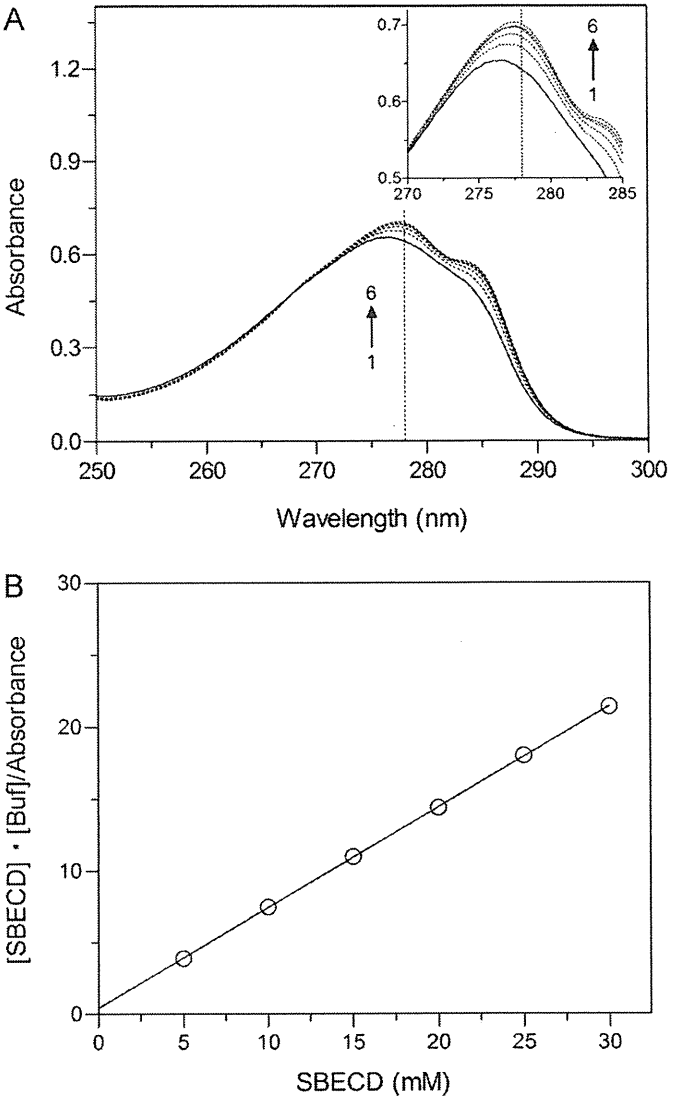

Fig. 4. Stoichiometry analysis of SBECD inclusion property for bufexamac. (A) UV spectral patterns of bufexamac (0.5 mM) with SBECD. Concentration of SBECD: (1) 5, (2) 10, (3) 15, (4) 20, (5) 25, and (6) 30 mM. (1) Solid line; (2)–(6) dotted line. (B) Scott's plot for interaction between bufexamac and SBECD by UV spectrometry.

3.4. Inhibitory effect of SBECD on ROS generation from bufexamac

Although SBECD complex with bufexamac could be formed, the influence of SBECD on the photochemical behavior of bufexamac is still unclear. Therefore, ROS generation from irradiated bufexamac (200 μM) co-existing with SBECD (ranging from 0 to 800 μM) was examined by ROS assay to clarify the possible transition of photoreactivity for bufexamac (Fig. 5). SBECD complexation led to suppression of superoxide generation from irradiated bufexamac in an SBECD-concentration-dependent manner. In detail, SBECD at concentrations of 20 and 100 μM exhibited significant reduction of superoxide generation from irradiated bufexamac by ca. 75 and 92%, respectively, and the generation of superoxide was negligible in the presence of SBECD at concentration of over 200 μM. On the basis of the data obtained, SBECD modulated the photoreactivity of bufexamac by forming an inclusion complex, and SBECD may attenuate bufexamac-induced phototoxic skin reactions by forming an inclusion complex when the complex is topically administered.

3.5. Photostability testing on bufexamac and its SBECD-inclusion complex

According to the ROS data, photoreactive and/or phototoxic potential of bufexamac is modulated by SBECD; this finding prompted us to clarify the photostability of bufexamac in SBECD. Solution-state photostability test using a solar simulator was

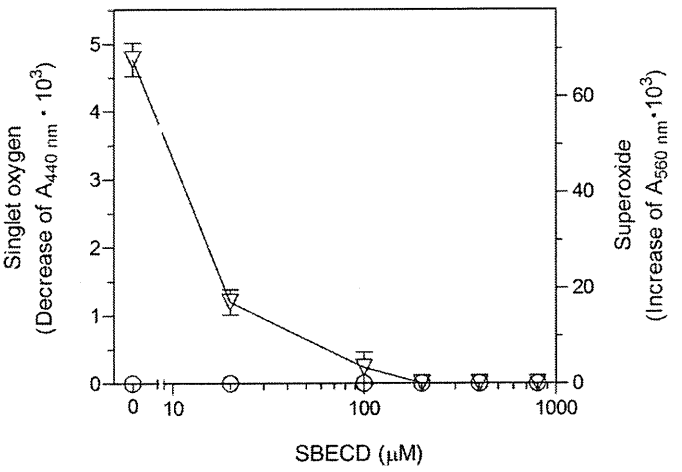

Fig. 5. Generation of ROS from irradiated inclusion complex of bufexamac with SBECD. SBECD was dissolved in 20 mM NaPB (pH 7.4) at the indicated concentrations with bufexamac (200 μM), and then exposed to simulated sunlight (30,000 lx). (○) singlet oxygen; and (▽) superoxide. Data represent mean ± S.D. of three experiments.

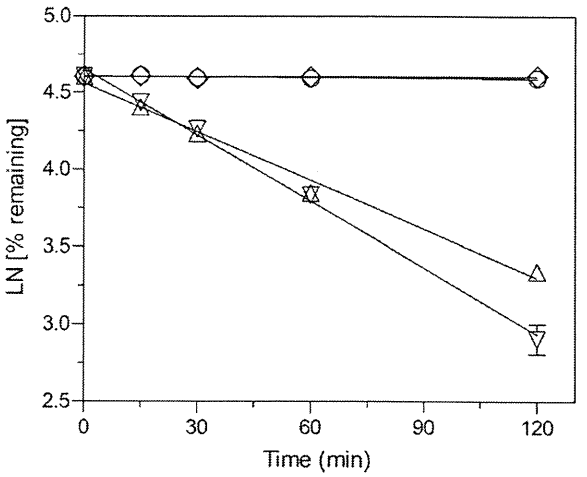

Fig. 6. Photodegradation profiles of bufexamac. Each sample was exposed to UVA/B (750 W/m^2) for the indicated periods, and the remaining bufexamac was evaluated by UPLC/ESI-MS. Bufexamac: (○) non-irradiated, and (▽) irradiated, and bufexamac–SBECD inclusion complex: (◇) non-irradiated, and (△) irradiated. Data represent mean ± S.D. of three experiments.

carried out on bufexamac with or without SBECD (Fig. 6). Degradation kinetics was calculated according to the following equation: $\ln A = \ln A_0 - kt$, where A is the remaining peak area of bufexamac, t is the time (min), and k is the slope (degradation constant). Both bufexamac solutions were stable without UV irradiation since the results of the remaining bufexamac were estimated to be almost 100% of initial bufexamac until 120 min in both bufexamac solutions. In contrast, solution-state bufexamac was rapidly photodegraded by exposure to UV, and the remaining bufexamac at 120 min was estimated to be ca. 18.3%. The solution-state bufexamac in SBECD was also photodegraded after UV irradiation, and the remaining bufexamac at 120 min was calculated to be ca. 28.2%. The degradation constants of bufexamac with and without SBECD were estimated to be 1.05×10^{-2} min^{-1} and 1.43×10^{-2} min^{-1}, respectively. There was ca. 30% reduction of the degradation constant of bufexamac by forming SBECD complexation; therefore, the photostability of bufexamac should be slightly improved by SBECD.

4. Discussion

In the present study, we first demonstrated that SBECD complexation was effective for controlling the phototoxicity of bufexamac. On the basis of the photobiochemical data, bufexamac generated superoxide; however, the photogenotoxic potential of bufexamac was not identified. SBECD inclusion complex of bufexamac was prepared, and the inclusion ratio was estimated to be 1:1 by a spectroscopic method. From the photochemical data on the inclusion complex, the photoreactivity of bufexamac might be modulated by equimolar SBECD.

Generally, CyDs are often applied for improving solubility, dissolution rate, bioavailability, and chemical stability, including hydrolysis oxidation and photodegradation of drugs [22,23]. In particular, β-CyD is considered a useful solubilizing agent because of its inclusion abilities; however, natural β-CyD has limited aqueous solubility due to relatively strong binding of the CyD molecules. To overcome this drawback, SBECD, an anionic β-CyD derivative, was synthesized for better solubilization than natural β-CyD, and it has been applied as a solubilizing agent for some pharmaceutics, such as ziprasidone, aripiprazole, and voriconazole [24].

On the basis of the ROS data, bufexamac was found to have photoreactivity, possibly leading to photodegradation and phototoxicity; however, the potent photogenotoxic risk of bufexamac was not observed in all the *in vitro* photogenotoxic assessment tools. Although the photogenotoxic risk of bufexamac was negligible, bufexamac should be indicative of photoreactivity mainly via type I photochemical reaction since bufexamac is topically used in clinical settings, and the phototoxic risk of bufexamac is recognized as one of its severe side effects. To attenuate the phototoxic potential of bufexamac, SBECD-based formulation was designed in the present investigation. On the basis of the physicochemical data, SBECD should form equimolar and stable inclusion complex with bufexamac. Photochemical properties of the inclusion complex were examined to clarify whether SBECD truly attenuated the phototoxicity of bufexamac. On the basis of the ROS data, generation of superoxide from bufexamac was completely inhibited by more than an equimolar concentration of SBECD. The photostability of bufexamac was also improved slightly by forming inclusion complex with SBECD owing to the ca. 30% reduction of the degradation constant of bufexamac. The results suggest that SBECD attenuated photoactivation of bufexamac and/or blocked interaction of excited bufexamac with oxygen owing to complexation with bufexamac. Overall, bufexamac in SBECD was found to be less photoreactive than bufexamac itself, and SBECD-based complexation might be effective for modulating the phototoxicity of bufexamac in terms of photosafety.

Topical application of chemicals on the skin provokes the concern about the occurrence of the phototoxic risk of the compounds because of direct exposure of the skin to both compounds and sunlight. Previously, Moore et al. reported that topically applied agents, such as ketoprofen, coumarin, and hydrocortisone, induced direct cutaneous phototoxicity [25]. According to the European Medicines Agency (EMEA) and the Food and Drug Administration (FDA) guidelines [26–28], topical application of compounds has been explicitly described as one of the conditions for testing chemicals; therefore, attenuation of the phototoxic risk of topically applied chemicals is required in terms of photosafety. Sunscreens are usually used to avoid drug-induced photodermatoses [25], and the present investigation suggested that CyD complexation may also be an effective approach for controlling the phototoxicity of topically administered drugs.

In conclusion, SBECD could inhibit ROS generation from irradiated bufexamac and slightly improve the photostability of bufexamac; therefore, the phototoxic risk of bufexamac could be reduced by SBECD complexation, and the SBECD-based formulation strategy might be effective for modulating the phototoxicity of bufexamac.

Acknowledgements

This work was supported in part by a Grant-in-Aid from the Food Safety Commission, Japan [No. 0807] and a Health Labour Sciences Research Grant from The Ministry of Health, Labour and Welfare, Japan.

References

[1] S. Onoue, Y. Tsuda, Analytical studies on the prediction of photosensitive/phototoxic potential of pharmaceutical substances, Pharm. Res. 23 (2006) 156–164.
[2] S. Onoue, Y. Seto, G. Gandy, S. Yamada, Drug-induced phototoxicity; an early *in vitro* identification of phototoxic potential of new drug entities in drug discovery and development, Curr. Drug Saf. 4 (2009) 123–136.
[3] C.S. Foote, Definition of type I and type II photosensitized oxidation, Photochem. Photobiol. 54 (1991) 659.
[4] D.E. Moore, Mechanisms of photosensitization by phototoxic drugs, Mutat. Res. 422 (1998) 165–173.
[5] F. Vargas, I. Martinez Volkmar, J. Sequera, H. Mendez, J. Rojas, G. Fraile, M. Velasquez, R. Medina, Photodegradation and phototoxicity studies of furosemide. Involvement of singlet oxygen in the photoinduced hemolysis and lipid peroxidation, J. Photochem. Photobiol. B 42 (1998) 219–225.

[6] L. Becker, B. Eberlein-Konig, B. Przybilla, Phototoxicity of non-steroidal anti-inflammatory drugs: *in vitro* studies with visible light, Acta Derm. Venereol. 76 (1996) 337–340.
[7] G. Viola, G. Miolo, D. Vedaldi, F. Dall'Acqua, *In vitro* studies of the phototoxic potential of the antidepressant drugs amitriptyline and imipramine, Farmaco 55 (2000) 211–218.
[8] S. Onoue, K. Kawamura, N. Igarashi, Y. Zhou, M. Fujikawa, H. Yamada, Y. Tsuda, Y. Seto, S. Yamada, Reactive oxygen species assay-based risk assessment of drug-induced phototoxicity: classification criteria and application to drug candidates, J. Pharm. Biomed. Anal. 47 (2008) 967–972.
[9] M. Partyka, B.H.A.H. Evans, Cyclodextrins as phototoxicity inhibitors in drugs formulation; studies on model systems involving naproxen and β-cyclodextrin, J. Photochem. Photobiol. A: Chem. 140 (2001) 67–74.
[10] G. Ragno, E. Cione, A. Garofalo, G. Genchi, G. Ioele, A. Risoli, A. Spagnoletta, Design and monitoring of photostability systems for amlodipine dosage forms, Int. J. Pharm. 265 (2003) 125–132.
[11] S. Sortino, S. Petralia, G. Condorelli, G. Marconi, Direct spectroscopic evidence that the photochemical outcome of flutamide in a protein environment is tuned by modification of the molecular geometry: a comparison with the photobehavior in cyclodextrin and vesicles, Helv. Chim. Acta 86 (2003) 266–273.
[12] M.A. Tomren, M. Masson, T. Loftsson, H.H. Tonnesen, Studies on curcumin and curcuminoids. XXXI. Symmetric and asymmetric curcuminoids: stability, activity and complexation with cyclodextrin, Int. J. Pharm. 338 (2007) 27–34.
[13] Y. Kurumaji, Photo Koebner phenomenon in erythema-multiforme-like eruption induced by contact dermatitis due to bufexamac, Dermatology 197 (1998) 183–186.
[14] S. Onoue, Y. Seto, A. Oishi, S. Yamada, Novel methodology for predicting photogenotoxic risk of pharmaceutical substances based on reactive oxygen species (ROS) and DNA-binding assay, J. Pharm. Sci. 98 (2009) 3647–3658.
[15] R.L. Scott, Some comments on the Benesi–Hildebrand equation, Rec. Trav. Chim. Pays B 75 (1956) 787–789.
[16] I. Kraljic, S.E. Mohsni, A new method for the detection of singlet oxygen in aqueous solutions, Photochem. Photobiol. 28 (1978) 577–581.
[17] M.A. Pathak, P.C. Joshi, Production of active oxygen species ($^1O_2$ and O_2^{-}.) by psoralens and ultraviolet radiation (320–400 nm), Biochim. Biophys. Acta 798 (1984) 115–126.
[18] T. Terui, H. Tagami, Eczematous drug eruption from carbamazepine: coexistence of contact and photocontact sensitivity, Contact Dermatitis 20 (1989) 260–264.
[19] S. Onoue, M. Ochi, G. Gandy, Y. Seto, N. Igarashi, Y. Yamauchi, S. Yamada, High-throughput screening system for identifying phototoxic potential of drug candidates based on derivatives of reactive oxygen metabolites, Pharm. Res. 27 (2010) 1610–1619.
[20] V.I. Ivanov, L.E. Minchenkova, A.K. Schyolkina, A.I. Poletayev, Different conformations of double-stranded nucleic acid in solution as revealed by circular dichroism, Biopolymers 12 (1973) 89–110.
[21] M. Otagiri, K. Uekama, K. Ikeda, Inclusion complexes of beta-cyclodextrin with tranquilizing drugs phenothiazines in aqueous solution, Chem. Pharm. Bull. 23 (1975) 188–195.
[22] T. Loftsson, M.E. Brewster, Pharmaceutical applications of cyclodextrins. 1. Drug solubilization and stabilization, J. Pharm. Sci. 85 (1996) 1017–1025.
[23] S. Scalia, R. Tursilli, N. Sala, V. Iannuccelli, Encapsulation in lipospheres of the complex between butyl methoxydibenzoylmethane and hydroxypropyl-beta-cyclodextrin, Int. J. Pharm. 320 (2006) 79–85.
[24] D.R. Luke, K. Tomaszewski, B. Damle, H.T. Schlamm, Review of the basic and clinical pharmacology of sulfobutylether-beta-cyclodextrin (SBECD), J. Pharm. Sci. 99 (2010) 3291–3301.
[25] D.E. Moore, Drug-induced cutaneous photosensitivity: incidence, mechanism, prevention and management, Drug Saf. 25 (2002) 345–372.
[26] The European Agency for the Evaluation of Medicinal Products, Evaluation of Medicines for Human Use, Committee for Proprietary Medicinal Products, Note for Guidance on Photosafety Testing, CPMP/SWP/398/01, 2002.
[27] The European Agency for the Evaluation of Medicinal Products, Evaluation of Medicines for Human Use, Committee for Proprietary Medicinal Products, Concept Paper on the Need for Revision of the Note for Guidance on Photosafety Testing, CPMP/SWP/398/01, 2008.
[28] United States Department of Health and Human Services, Food and Drug Administration, Center for Drug Evaluation and Research (CDER) Guidance for Industry, Photosafety Testing, 2002.

日薬理誌（*Folia Pharmacol. Jpn.*）**138**，99～102（2011）

薬理学における動物実験代替法研究の重要性

大野　泰雄

要約：薬理学研究における薬物の作用標的の解析や医薬品候補物質の研究等にin vitro試験法が広く利用されている．しかし，様々な理由で，in vitroで得られた結果が必ずしもin vivoで再現できないことが多く，in vivo動物実験を欠かすことができない．平成23年3月に予定していた薬理学会年会においても，多数の動物実験結果が発表される予定であった．一方，動物実験については，市民による反対運動もあり，3Rsの原則に則り適正に実施することが法的に求められている．また，世界的に代替法の開発・評価を専門的に行う国立の機関も多く構築されている．薬理学が今後も社会のサポートを得，継続して発展していくためには，関連法規制を遵守し，動物実験を行う機関，施設，機材および人材を整備し，代替法について研究者教育を行うとともに，それらの適切性について第三者により評価を受けることが重要である．これは一研究者により対応できることではなく，研究機関が組織として対応して初めて達成することが可能である．

はじめに

近代における生物科学発展の多くは動物実験により支えられてきた．しかし，動物の福祉や権利の立場から動物実験への批判も多く，動物実験代替法が検討されてきた．

Russell と Burch（1959）(1) の定義によれば，動物実験代替法（代替法）とは科学研究や教育，毒性試験，生産等の目的のために動物を用いる方法を動物を用いない方法に置き換えること（Replacement）であり，動物使用数の削減（Reduction）や動物使用に伴う苦痛の削減（Refinement）を含むものである．この考えは日本も含め，国際的に広く受け入れられている．

代替法開発はもともと動物愛護の精神に根ざすものであるが，無駄な動物実験の廃止や多数の新規化学物質の経済的な安全性評価，極めて毒性の強い可能性のある化学物質の毒性を動物実験で調べることに伴う危険の回避，また，ヒトへの外挿のために必要な毒性発現機序に関する情報の確保のためにも有効である．新しい代替法の開発は独創性のある研究への道を開くのみならず，遺伝子突然変異を検出するAmes' 試験のように，発がん機構解明だけでなく，発がん物質スクリーニングのために行政的に広く使われ，発がん物質の管理に大きな貢献をしたものもある．

一方，新しい試験法，特に従来の動物実験に替わるものとして新規に開発された試験法を受け入れるためには，適切なバリデーションを行い使用目的に合致していることを確認する必要がある．特に，既存の毒性試験法を新しい試験法（代替法）に置き換えることにより，医薬品や農薬等，化学物質の安全性評価のレベルが低下することは許されない．従って，新規安全性試験法を公的な試験法として受け入れるためには，複数の機関により，GLPに準じて実施されたバリデーションにより，その利点と限界が明確にされ，既存の方法と比べ同等以上の有用性があることが，第三者により確認されなくてはならない．具体的なバリデーションの方法や行政的受入の基準については，小野（1994）(2)，大野（2004）(3)，OECD（2005）(4) などを参照されたい．

1．動物実験代替法に関わる機関

代替法の研究は欧米では早くから行われており，イギリスでは医学分野における実験動物を他のものに置き換えるための基金（FRAME）が1969年に，米国では1981年にジョンズホプキンズ大学に代替法センターが開設された．日本では1982年に現在の動物実験

キーワード：動物実験代替法，薬理学
国立医薬品食品衛生研究所（〒158-8501 東京都世田谷区上用賀1-18-1）
E-mail: ohno@nihs.go.jp　原稿受領日：2011年6月1日，依頼原稿
Title: Alternatives to animal experiments in pharmacology.　Author: Yasuo Ohno